

NSERC Form 101, Part II

1 Introduction

TWIST, the TRIUMF Weak Interaction Symmetry Test, proposes to measure the parameters describing the energy and angular (with respect to muon spin) distributions and correlations of positrons (e^+) from positive muon (μ^+) decay. Historically, they are known as the Michel parameters (after Prof. L. Michel [1]), and although more general and modern descriptions exist [2], they offer a compact and convenient prediction of the electroweak interaction in muon decay.

The proposal describes the methods by which the experimental precision can be improved by more than one order of magnitude for the Michel parameters ρ , δ , and $P_\mu\xi$; we will perhaps determine an improved value of η as well. It describes the physics motivation and the significance of the detailed objectives of the collaboration throughout the lifetime of the experiment, the spectrometer which has been constructed to make the measurements, and how each component functions to provide the precision required. It summarizes the recent progress we have made as a group toward our objectives, and how our students, research associates, and external collaborators contribute to the tasks involved.

1.1 Responsibilities

TWIST is based substantially in Canada, with three of the current total of four students in the collaboration, four of the current total of five post-docs, and 19 of the 28 current total faculty and research scientists. As well, the Canadian team benefits from an outstanding professional staff. The Canadian team leads the experiment, with individuals committed to making contributions shown in Table 1. It is clear from the list of commitments that the Canadian team plays the central role in the experiment.

The *TWIST* group benefits from a strong theoretical support at the University of Alberta, who provide calculations of second-order radiative corrections. This group, led by Prof. Andrzej Czarnecki, works on the radiative corrections to provide theoretical input to the interpretation of *TWIST* results.

2 Physics Motivation

The Standard Model of the strong, weak and electromagnetic interactions, based on the gauge group $SU(3)_C \times SU(2)_L \times U(1)_Y$, has proven to be remarkably successful in describing the existing experimental observations. At present, there exist no experimental results that deviate from its expectations, with the exception of neutrino oscillations which in any case result from a simple extension to the mass matrices. However, the Standard Model is universally believed to be an incomplete theory of nature in spite of its many successes, and many extensions have been proposed.

Normal muon decay $\mu \rightarrow e\nu\bar{\nu}$ is an ideal system with which to investigate the space-time structure of the weak interaction. This comes about because the purely leptonic nature of this decay eliminates any uncertainties due to the internal structure of the particles or contributions from other interactions. For example, the Michel spectrum gives a model independent description of the energy and angular distributions of the e^\pm emitted in the decay of polarized μ^\pm . In the limit where radiative corrections are neglected this spectrum is given by:

$$\frac{d\Gamma}{x^2 dx d(\cos\theta)} \propto 3(1-x) + \frac{2}{3}\rho(4x-3) + 3\eta x_o \frac{1-x}{x} \pm P_\mu\xi \cos\theta [1-x + \frac{2}{3}\delta(4x-3)] \quad (1)$$

Grant Signator	Time Commitment				Topical Commitment
	Percentage / Hours per month				
	2003	2004	2005	2006	
P. Depommier	40/60	40/60	40/60	40/60	depolarization, radiative corrections
J. Doornbos	50/90	25/45	25/45	25/45	muon beams, polarization
D.R. Gill	100/200	100/200	100/200	100/200	analysis group leader
M. Hasinoff	30/45	30/45	30/45	30/45	wire chamber response
R. Helmer	20/40	20/40	20/40	20/40	muon beams, production target
R. Henderson	50/100	50/100	50/100	50/100	TEC, drift, proportional chambers
P. Kitching	50/70	50/70	50/70	50/70	alignments, mechanical systems
J. Macdonald	35/70	35/70	35/70	35/70	solenoid, cryogenics
G.M. Marshall	100/180	100/180	100/180	100/180	group leader, muon beams
E.L. Mathie	30/35	50/60	50/60	50/60	WC corrections, alignments
A. Olin	40/80	40/80	40/80	40/80	software group leader
J.M. Poutissou	90/50	90/50	90/50	90/50	trigger, Monte Carlo
R. Poutissou	50/90	50/90	50/90	50/90	DAQ, code management
B. Shin	80/80	80/80	80/80	80/80	software
G. Stinson	50/45	50/45	50/45	50/45	beam optics calculations
R. Tacik	35/70	50/100	65/130	65/130	software and analyses
Total FTEs	8.50	8.60	8.75	8.75	
Post-Docs					
Y. Davydov	100/180	100/180	100/180	100/180	chamber development
M. Quraan	100/180	100/180	100/180	100/180	software coordination
S.C. Wang and replacement	100/180	100/180	100/180	100/180	alignment, calibrations
Grad Students					
A. Gaponenko (PhD)					energy calibration, δ
B. Jamieson (PhD)					depolarization, $P_\mu\xi$
R. MacDonald (PhD)					beams, ρ
Research Physicist					
P. Gumplinger					Monte Carlo
Professional Staff					
W. Andersson					mechanical engineering
C. Ballard					solenoid, cryogenics
B. Evans					monitoring electronics
D. Evans					field mapping
W. Faszler					wire chambers, QC
D. Maas					electronics
K. Olchanski					systems, software, tracking
R. Openshaw					gas systems
J. Schaapman					electronics
G. Sheffer					electronics
J. Soukup					mechanical engineering

Table 1: Summary commitments of Canadian participants.

where θ is the angle between the muon polarization and the outgoing electron direction, $x = E_e/E_{max}$, $x_o = m_e/E_{max}$, and P_μ is the muon polarization. The three Michel parameters[1] ρ , ξ and δ completely determine the spectrum if neither the neutrinos nor the spin of the outgoing electron are observed. A fourth parameter η contributes to the energy spectrum when the electron mass is included in the analysis.

In the Standard Model with pure $(V - A)$ coupling, the four Michel parameters take specific values, as shown in Table 2. The current experimental results [3] are consistent with these

values. *TWIST* will determine ρ , δ , η , and $P_\mu\xi$ with significantly improved precision providing an excellent opportunity to observe physics outside the Standard Model if one or more of the measured Michel parameters differs from its expected value.

	Accepted Value	Standard Model Value	<i>TWIST</i> Precision
ρ	0.7518 ± 0.0026	$\frac{3}{4}$	± 0.0001
δ	$0.7486 \pm 0.0026 \pm 0.0028$	$\frac{3}{4}$	± 0.00014
$P_\mu\xi$	$1.0027 \pm 0.0079 \pm 0.0030$	1	± 0.00013
η	-0.007 ± 0.013	0	± 0.003

Table 2: The accepted values of the Michel parameters[3] along with the Standard Model values.

On the other hand, if the ultimate *TWIST* results are consistent with the Standard Model, they will permit us to set far more stringent limits than possible at present on those extensions to the Standard Model that influence the space-time structure of the weak interaction. For example we will obtain new upper limits on the possible electroweak couplings from the above constraints. These anticipated new limits, shown in columns 2-5 of Table 3, were established by varying the magnitudes of non-($V - A$) coupling constants (as defined in [2, 3]) independently from zero up to the current limit for each coupling, and the relative phases in the interference terms were varied from 0 to π . For each combination of couplings and phases which satisfied the constraints, maximum values of the couplings were found. In the first column, the limits as quoted by the Particle Data Group[3] are given.

In the most general case (D) - models which allow any Vector, Axial vector, Scalar, or Tensor derivative-free interactions - limits on all of the RR and LR couplings are improved over the current values while the RL and LL limits are not improved. However, since very few extensions of the standard model include both scalar and tensor couplings, three additional cases were studied:

- A) only vector and axial vector couplings are allowed,
- B) all but scalar couplings are allowed, and
- C) all but tensor couplings are allowed.

In all these latter cases, the analysis is greatly simplified because there are fewer couplings to vary and because the interference terms between scalar and tensor couplings in ρ , ξ , and δ disappear, allowing one to take advantage of the positive-definite nature of many of the terms.

Case A is a minimal extension of the standard model, in which only three independent vector coupling constants are needed. In this case the limit on the total deviation from $V - A$ is quite stringent, as seen by the deduced lower limit on g_{LL}^V . This leads to significant new limits on the existence of right-handed currents in left-right symmetric theories. Assuming that the right-handed neutrinos are light, non-zero g_{RR}^V is dependent upon the mass of the right-handed vector boson W_R , while non-zero g_{RL}^V and g_{LR}^V indicate mixing between the intermediate vector bosons W_L and W_R . A measurement of the parameters ξ and ρ will therefore set limits on both the left-right mixing angle ζ and the right-handed boson mass M_R . *TWIST* will actually measure

	Current Limits	<i>TWIST</i> (A)	<i>TWIST</i> (B)	<i>TWIST</i> (C)	<i>TWIST</i> (D)
$ g_{RR}^S $	<0.066	—	—	<0.020	<0.045
$ g_{RR}^V $	<0.033	<0.012	<0.014	<0.013	<0.022
$ g_{LR}^S $	<0.125	—	—	<0.027	<0.046
$ g_{LR}^V $	<0.060	<0.012	<0.013	<0.012	<0.018
$ g_{LR}^T $	<0.036	—	<0.009	—	<0.013
$ g_{RL}^S $	<0.424	—	—	—	—
$ g_{RL}^V $	<0.110	<0.012	<0.012	<0.011	—
$ g_{RL}^T $	<0.122	—	<0.008	—	—
$ g_{LL}^S $	<0.55	—	—	—	—
$ g_{LL}^V $	>0.96	>0.99977	>0.99953	—	—

Table 3: Upper limits (90% CL) for weak coupling constants with current limits taken from [3]. Anticipated improved limits set by *TWIST* based on measurements of ρ , ξ , and δ assume (A) V, A couplings only, (B) V, A and T couplings, (C) V, A and S couplings or (D) most general (V, A, S and T) derivative-free couplings.

the quantity $P_\mu\xi$, and not ξ and P_μ separately. Since the surface muons employed by *TWIST* are produced in pion decay at rest, the value of the μ^+ helicity is equal to the ν_μ helicity, taken to be negative. For a measured value of $P_\mu\xi$ the allowed region in mixing angle-mass space is limited by [4]

$$\frac{1 - P_\mu\xi}{4} = \zeta^2 + \frac{M_L^4}{M_R^4} + \zeta \frac{M_L^2}{M_R^2}. \quad (2)$$

Using this relation, the 95% CL limit for $P_\mu\xi$ from *TWIST* yields a lower limit for the W_R mass

$$M_R > 819 \text{ GeV}/c^2$$

and a limit on the range of ζ

$$-0.00961 < \zeta < 0.00832 .$$

When comparing these limits to those from other experiments it must be recalled that most experimental tests of left-right symmetric theories are sensitive to the form assumed for the right-handed CKM matrix. Muon decay studies have essentially no sensitivity to such assumptions. Thus limits established by *TWIST* will be complementary to, for example, the recent result from the D0 experiment: $M_R > 720 \text{ GeV}$ for $V_{ud}^R \approx 1$ ($V^R = V^L$)[5]. A *TWIST* result that indicated $M_R < 720 \text{ GeV}$ would raise questions regarding the D0 assumption about V_{ud}^R .

A recent report [6] from the CDF collaboration describes a search for a W' decaying to tb pairs. No signal was found, allowing them to exclude the particle in a mass range of 225 to about 550 GeV/c^2 , under certain model assumptions.

The above discussion was predicated on the assumption that the right-handed neutrinos are light, so they are not kinematically suppressed in muon decay. In this limit, lepton universality

requires $|g_{LR}^V| = |g_{RL}^V|$, so δ retains its Standard Model value of 0.75. Alternative patterns for the three vector coupling constants appear in left-right symmetric models if one or both of the right-handed neutrinos are heavy. For example, if the right-handed muon neutrino is light, while the right-handed electron neutrino is heavy, g_{RR}^V and g_{RL}^V must both remain zero, while g_{LR}^V can be non-zero. This changes the relationships between ξ and ρ and ζ and M_R , and permits δ to deviate from its Standard Model value. A similar situation arises if only the right-handed electron neutrino is light. In fact, in this case, Herczeg noted [4] that $P_\mu \xi \delta / \rho$, the quantity measured by Strovink *et al.* [7][8], must remain identically equal to its Standard Model value of 1, while ξ , δ , and ρ may separately deviate from their respective Standard Model values. *This emphasizes the importance of a comprehensive investigation of all of the Michel parameters over a broad energy range, as will be provided by TWIST.* If both of the right-handed neutrinos are heavy, g_{LR}^V , g_{RL}^V and g_{RR}^V must all remain zero.

A more speculative model [9], based on the existence of a scalar particle which would mediate a lepton-number-violating decay of the muon, has been proposed recently in an attempt to reconcile the LSND result with other observations. The mechanism would give rise to a difference in ρ at the level of 10^{-3} .

The above discussion, while limited, indicates that an improved measurement of the Michel parameters of muon decay will have a significant impact on our understanding of the space time structure of the electroweak interactions and will impose strict limits on new particles and proposed extensions of the Standard Model.

3 The TWIST Experiment

The TWIST experiment uses a highly polarized surface muon beam, from the decay of positive pions (π^+) produced by a high intensity proton source (the TRIUMF cyclotron). The pions that produce surface muons decay at thermal energy near the surface of a small production target. The high polarization arises from the two-body decay of the spinless pion into the muon and a near-massless neutrino (ν_μ). The positive muons (μ^+) are transported by a conventional dipole-quadrupole magnetic system (the M13 beam line) in vacuum to an achromatic double (horizontal and vertical) focus near the entrance to a superconducting solenoid. They pass through a thin scintillator in air and into a stack of low mass planar drift chambers inside the solenoidal field to stop in a thin target at the center of the stack and also at the center of the uniform field. Throughout this transport, the muon spin direction is affected very little and the high polarization remains. Furthermore, the high solenoidal field effectively locks the spin so that it does not significantly relax or diminish in the materials used.

The muon decays predominantly to a positron (e^+) and two neutrinos (ν_e and $\bar{\nu}_\mu$). While the neutrinos are unobserved, the high precision tracking of the positron through the detector planes within the field yields both its initial momentum and direction. The distributions of momentum and direction can be compared with high precision to the predictions of the Standard Model for purely leptonic decay.

3.1 Spectrometer

The TWIST spectrometer, shown in Fig. 1, consists of a 2 T superconducting solenoid (originally employed for whole-body medical MRI) containing a stack of 44 precision planar drift chambers and 12 proportional chambers. A minimum bias trigger is obtained from a thin (250 μm) plastic scintillator at the entrance to the chamber stack.

The muons are stopped and decay at the axis of the highly symmetrical detector system. The arrangement allows the simultaneous measurement of nearly the entire spectrum, allowing the extraction of the Michel parameters from data obtained under consistent conditions.

The following important points should be noted:

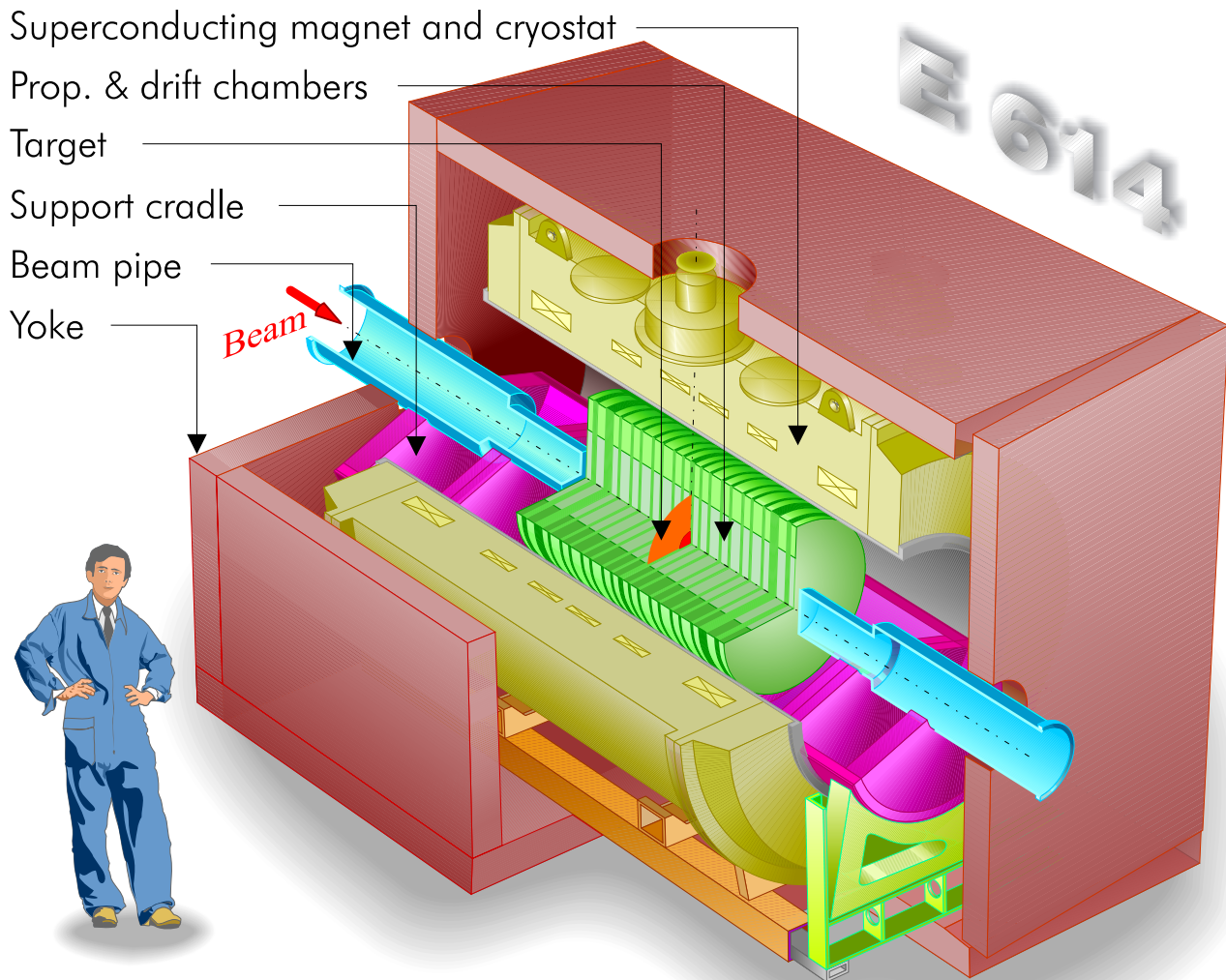


Figure 1: The *TWIST* spectrometer.

- The large acceptance of the spectrometer allows the coverage of the entire spectrum, including the endpoint energy. This means that it is possible to calibrate the energy scale without altering the magnetic field or other properties of the device.
- The device is extremely precise due to high precision assembly techniques and quality control (QC), as described in section 3.2.
- The use of planar drift chambers results in a very simple energy loss described by

$$\frac{dE}{dz} = \frac{dE(\cos(\theta) = 1)}{dz \cos(\theta)} \quad (3)$$

As a result, average corrections for energy loss are very reliable.

- The device has very low mass. Approximately $15 \text{ mg} \cdot \text{cm}^{-2}$ of material are in the path of the outgoing positrons prior to the tracking volume of the detector. Energy loss within the tracking volume is on average $7 \text{ keV}/\cos(\theta)$ per orthogonal chamber pair (UV) module.

Considerable progress was made this past year in refining the TWIST magnetic field and in obtaining more detailed understanding of the field and the magnet itself. After the engineering run in the fall of 2001, additional field symmetry studies were carried out with the “6-Way” Hall probe array, a device with Hall probes at the face centers of a 40 cm cube. In these studies, both the field profiles from the probes, as well as axial force measurements from load cells mounted inside the solenoid vacuum chamber on the longitudinal coil suspension struts, were used to determine the optimum location of the cryostat, and thus the coil array within the steel yoke. This practical iterative approach overcomes the limitations imposed by incomplete detailed knowledge of parameters such as the iron permeability and precise physical location of the coils and amp-turn distributions.

These studies determined an optimum placement of the cryostat 1.25 mm upstream and 8 mm above the geometrical centre of the iron. Both adjustments are within reasonable expectations for the mechanical dimensions of the coil. In particular, the rather large vertical displacement is consistent with internal measurements of the coils with respect to the cryostat, taken while the cryostat was open for repairs of the supporting struts in 2001.

In January – April 2002 the final assembly, installation, commissioning and alignment of the full field mapper for the magnet were carried out. The mapper consists of a tubular beam which carries the Hall and/or NMR probes, which can be moved axially and rotated about its axis by a drive system mounted downstream of the magnet. The tubular beam also rides on a carriage on the detector support tracks inside the magnet, and the full range of travel and mounting options allow mapping of the full spectrometer volume occupied by the detector array, as well as the upstream beam path from the last beamline element to the detector array. The mapper motion and data acquisition is computer controlled.

Seven Hall probes were mounted on a radial arm to cover the cylindrical volume occupied by the spectrometer wire chamber array: the radial range was from 0 to 247.7 mm in 41.3-mm steps and the arm was moved through the axial range $-650 \text{ mm} < z < 650 \text{ mm}$ in 50-mm steps and in azimuthal angle $0 < \phi < 345 \text{ deg}$ in 15-deg steps. Additional maps in finer z -steps were taken near the ends of the cylindrical region. The Hall probes provided field measurements with a reproducibility of $\pm 0.2 \text{ G}$, although the probe-to-probe relative calibration was only $\pm 1 \text{ G}$.

In order to obtain the required precision in probe-to-probe calibration as well as an absolute field calibration, several measurements and maps were carried out with an NMR probe. One set of these measurements was obtained simply by positioning the NMR probe by hand as close as possible to each of the Hall probes. A much more extensive set of NMR measurements was carried out by mounting the probe on the same tubular beam as the Hall probes and moving the probe through a mapping program under computer control. These maps were repeated with the probe mounted at radii corresponding to the Hall probes #1, #3, and #5. The region mapped

by NMR was constrained by the physical size of the probe, and by the region in which the field was sufficiently uniform for the NMR signal to lock.

Extensive mapping data were taken with the nominal field of 2 T. Additional maps with fewer NMR measurements were taken at 1.96 T and 2.04 T in order to study the systematics of field uniformity near the operating point. The magnet yoke was designed for optimum field uniformity at 2 T where the endplates, used to shape the radial field components for the incoming muon beam, are heavily saturated. At lower fields, the region of adequately uniform field diminishes.

A major goal of the field analysis is ultimately to reproduce the measured field using the Vector Fields OPERA simulation program. This allows a coherent use of the mapping data to minimize the effect of measurement artifacts such as unphysical fluctuations and calibration errors. If successful, it provides a more elegant method of interpolating between measurement coordinates for particle tracking analysis than, say, a phenomenological polynomial fit. Finally, the comparison to OPERA provides a powerful tool to study field characteristics and to attribute the observed imperfections to likely physical characteristics of the coil and steel yoke.

The analysis has provided some very promising initial results, some of which are illustrated in Fig. 2. On the left is shown the difference between the measured values and the OPERA values for B_z along the z axis, where OPERA uses the nominal characteristics for the coil. Of particular note is an upstream-downstream asymmetry which is inconsistent with a “perfect” coil. On the right is shown the same comparison with an OPERA calculation in which small ($\sim 0.2 - 2\%$) adjustments to the coil amp-turn distributions in three of the six coil assemblies have been made. Marked improved agreement is evident, and we are encouraged that it will be possible to represent the true spectrometer field with an OPERA calculation, perhaps with a small correction term. The OPERA comparison was used also to assess the presence of residual coil position asymmetries. There is no evidence for a z asymmetry and the x, y centering is better than ± 2 mm.

During the next major shutdown, further mapping is planned, first to check consistency with the maps taken this year, and then to map in detail the upstream region where influence on the incoming muon beam and depolarization effects are important to understand.

The TWIST collaboration gratefully acknowledges the efforts of Doug Evans, Dave Morris, members of the Experimental Support and Beamlines group and co-op student Amir Ahmadi in mapping the magnet. Another excellent co-op student, Roberto Armenta, developed remarkable expertise and insight in applying the OPERA package to analysing the data.

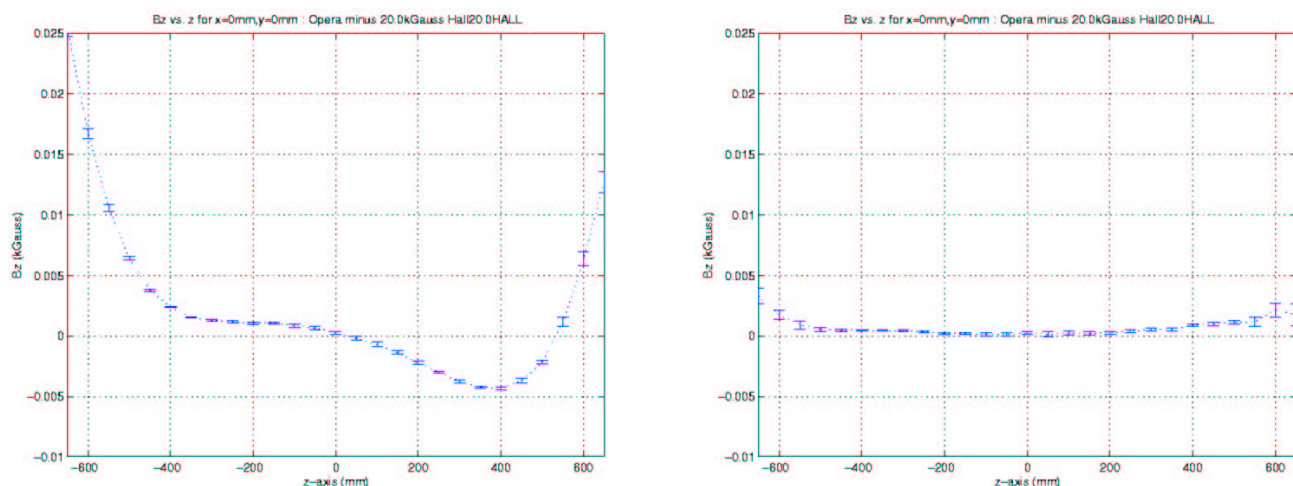


Figure 2: B_z vs. z plots for OPERA simulations minus the measured map (both nominal 2 T). On the left is the nominal “perfect” coil geometry in OPERA; on the right, small corrections to the coil were introduced to reproduce the measured field characteristics.

3.2 Detectors

A schematic view of a typical wire chamber plane is shown in Fig. 3. The DCs use a gas with a low drift speed (DME) to optimize tracking resolution, while the PCs use a gas with a high drift speed (CF₄/Isobutane) to optimize timing.

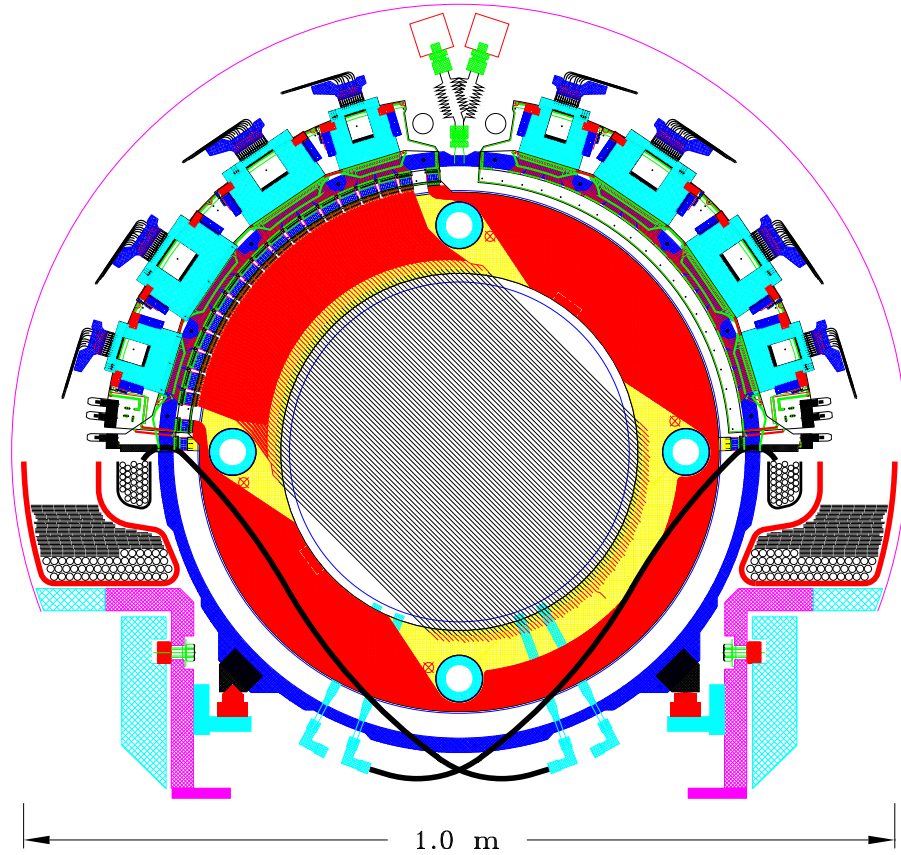
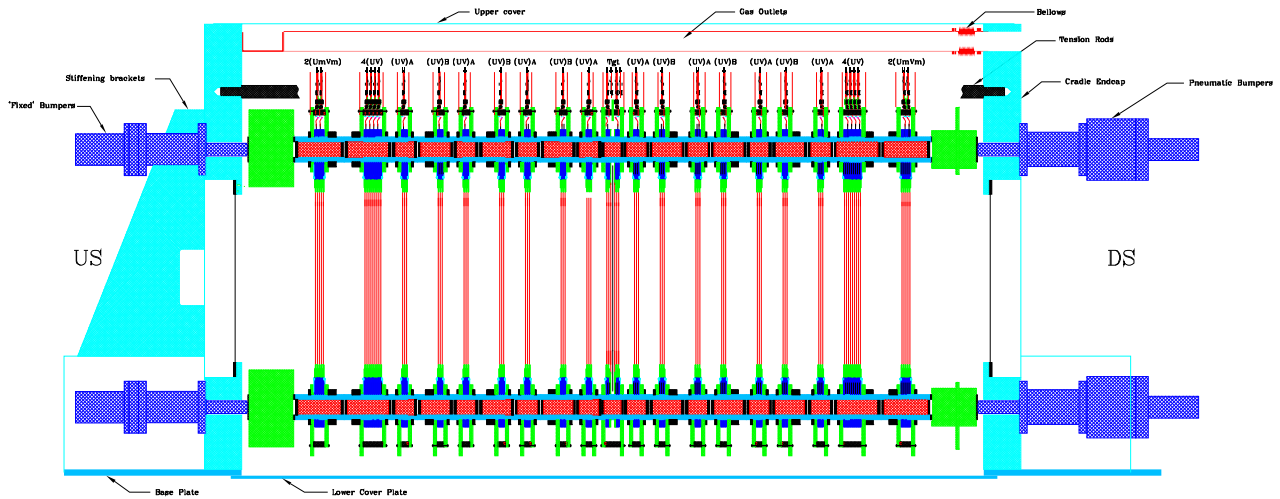


Figure 3: Schematic of one detector plane.

The wire planes are strung on glass frames which are referenced to a column of ceramic-glass citals, as shown in Fig. 4. These citals have a negligible coefficient of thermal expansion, and have been ground to high precision, allowing the spacing between any two wire planes to be defined to within a few microns on average.

In order to achieve the proposed precisions of Michel parameters, specific requirements must be met for chamber resolution, precision of chamber construction, and precision of assembly. Monte Carlo studies showed that the random rms error in wire position within the plane should not exceed $20 \mu\text{m}$, while the precision in wire pitch should be less than $\pm 2 \mu\text{m}$. The precision of the z position of wire planes due to accumulated errors should not exceed $\pm 2 \mu\text{m}$ per 4 mm (*i.e.*, per wire plane thickness) of detector length; in other words, the total detector length of about 120 cm long should be known with precision better than $600 \mu\text{m}$. At the same time, the amount of material in the detector should be minimized in order to decrease multiple scattering and energy loss of positrons from muon decay.

The TWIST spectrometer is comprised of wire chamber planes with 2 mm or 4 mm anode wire pitch. Although drift times are recorded for both types of planes, we refer to the 2 mm pitch planes as proportional chambers (PC), while those with 4 mm pitch are referred to as drift chambers (DC). The reason for this is that 4 mm pitch DC planes are used for track



TWIST Spectrometer

Figure 4: The *TWIST* detector stack. The muon beam enters from the left, and stops in a target at the center of the stack. From the left, the stack consists of 4 proportional chambers, a dense array of 8 drift chambers, 14 more drift chambers, two more proportional chambers, and the stopping target. The pattern is repeated symmetrically from the other end.

reconstruction while the 2 mm pitch PC planes are mainly used for fast timing, preliminary event topology definition, and for measurement of energy loss in planes near the target. The spectrometer consists of 44 DC planes, 4 target PC planes (2 on each side of the target), and another 8 PC planes (4 at the extreme upstream (US) end and 4 at the downstream (DS) end of the chamber stack). The planes are arranged along the z (beam and magnetic field) direction. If y is taken as vertical (up) and x is the horizontal direction to define a right handed system, the wires are parallel to directions u and v such that the (u, v) system is rotated by $\pi/4$ from the (x, y) system.

Each plane is constructed on a circular glass frame with inner diameter about of 40 cm. Four ceramic glass rings with thickness of $4,000 \pm 0.5 \mu\text{m}$ are key parts of each chamber plane. Surfaces of the ceramic glass rings act as reference positions for the wire grid and cathode foil.

All wire chambers have $15 \mu\text{m}$ diameter gold plated W(Re) sense wires. The DCs have 80 sense wires plus 2 guard wires on each side. There are two types of PCs. Full size US and DS PCs have 160 sense wires with 3 guard wires on each side; these PCs have 32 individual central sense wires while the remainder are ganged in groups of 4 wires. The target PCs, however, have 48 sense wires with 3 guard wires on each side; since part of their function is to define beam particles entering and exiting the target, and since the solenoidal field confines the low emittance beam particles to small radii, more wires are not necessary. In the magnetic field, decay positrons are detected by the PC wires for decay angles $|\theta - \pi/4| > 1^\circ$. All planes have 2 mm anode-cathode gaps. Cathodes are made from $6.35 \mu\text{m}$ thickness mylar, aluminized on both sides.

While the fully instrumented spectrometer requires 44 DC planes, 4 target PC planes and 8 PC planes, approximately 35% more planes were manufactured during the mass production, to serve as spares. A total of 56 DC planes, 12 PC planes and 8 target PC planes were produced. Quality control was carried out during all steps of chambers fabrication. This was essential to ensure reproducible results during mass production. All chamber mechanical parameters

(dimensions of components, wire tensions, positions, *etc.*) were checked during production and stored in a data base.

During production, a tension of 35 g was applied to all sense wires. Measured wire tensions are in the range of 30-31 g, the difference being due to friction of wires on the winding equipment. Fig.5 presents a histogram of the measured tensions of all 6784 sense wires on all DCs and PCs.

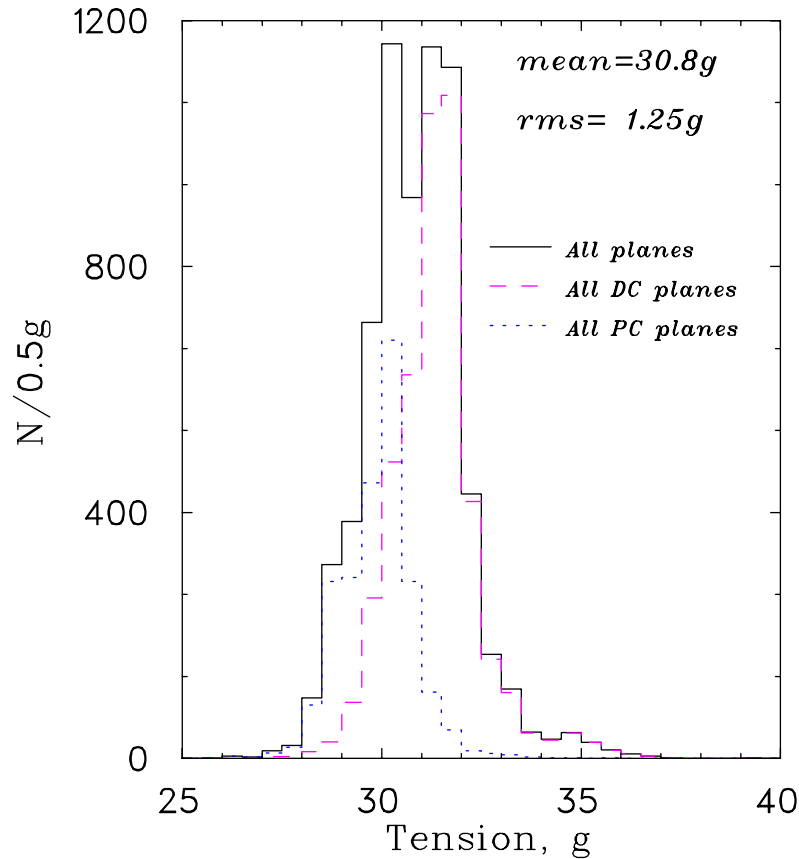


Figure 5: Tension of sense wires, for total of 6784 wires from all DCs, PCs and target PCs. Distributions for 4480 DC sense wires and 2304 PC wires are shown as well.

Two-dimensional wire positions (u or v and z) were measured for each plane after wire stringing. A travelling microscope based on two CCD cameras was used to measure wire positions; one CCD camera observed the wire displacement in u (or v), viewing from the z direction, while the second one simultaneously measured the displacement in the combination of u (or v) and z by viewing the wire at $\pi/4$ from the z direction. The estimated precision of the measuring system is about $1.5 \mu\text{m}$, based on comparison with a precision glass rule. Wire locations were determined near either end of a wire, about 10 cm from the center of the wire. For a wire plane, typical rms (σ) deviations of wire position from ideal are in the range of $2.5\text{-}5 \mu\text{m}$ on the DCs and PCs. Figure 6 shows the distribution of the σ at the wire center for the planes of each of 50 DCs. The values for centers were calculated from measurements of wire positions near the ends of wires. In the worst case, $\sigma = 4.13 \mu\text{m}$, much better than specification requirements.

A similar distribution of rms deviations for centers of wires on PC and target PC planes is presented in Fig.7, including data for 20 planes. In the worst case, $\sigma = 3.53 \mu\text{m}$, which is also much better than required.

The average measured wire pitch of 50 DC planes is 3.99995 ± 0.00001 mm and is much better than the required specification.

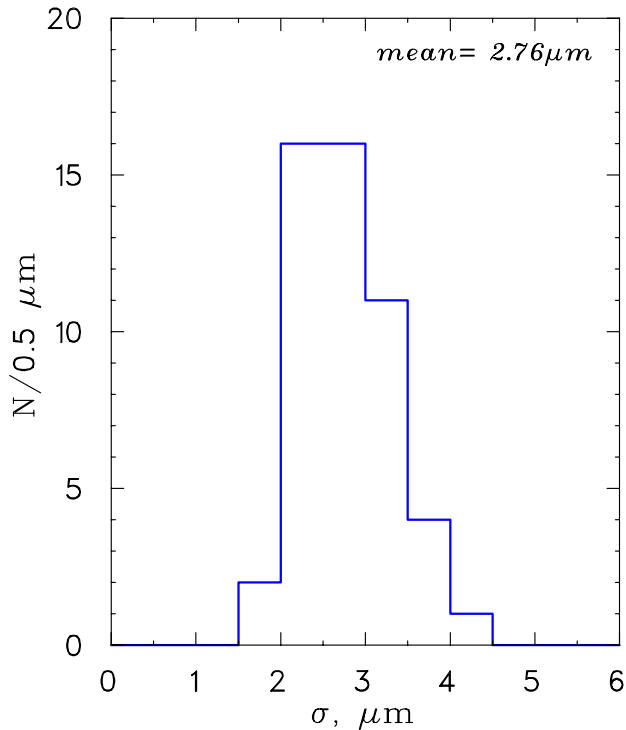


Figure 6: Distribution of precisions of wire positions (rms deviations σ) for centers of wires of 50 DC planes.

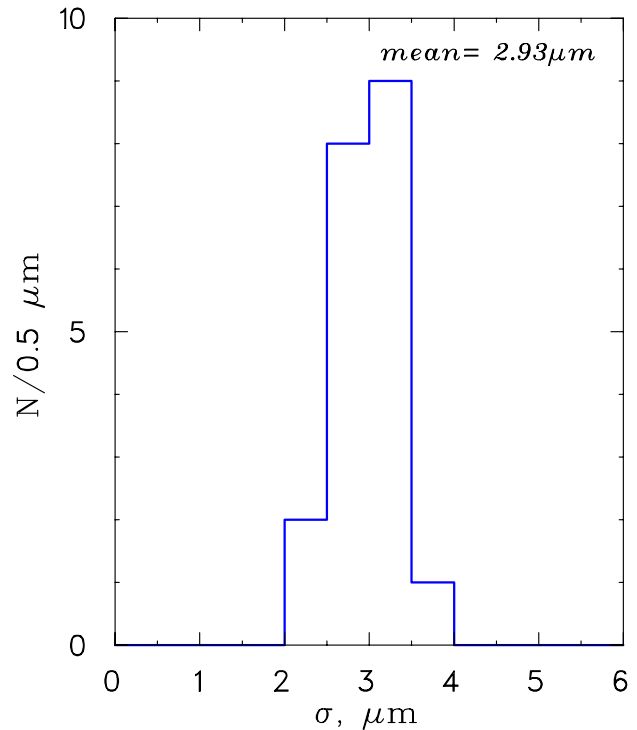


Figure 7: Distribution of precisions of wire positioning (rms deviations σ) for 12 PC and 8 target PC planes.

The results show that our winding equipment provided high quality and good reproducibility for wire plane production during a production period of almost 24 months. Moreover, the winding equipment enabled replacement with precision of a few microns of individual wires which were out of range or were broken due to cleaning. These excellent results have been achieved despite the participation in chamber production of about 20 people with different levels of experience.

As mentioned earlier, the wire planes were mounted in modules. Planes were placed one after another with wires in alternating u and v directions, using the ceramic glass ring surfaces for reference. A plane without wires served as the last cathode foil of a complete module. The planes were placed into gas boxes made of G10. Ceramic rings of 40 mm and 20 mm thickness were glued into the G10 disks. All planes and/or gas boxes touch only via ceramic ring surfaces. Thicknesses of all ceramic glass rings are known with precision better than $0.5 \mu\text{m}$ and are stored in a data base. When compressed, the assembly has precise anode-cathode distances both within each plane of the module and between planes. The outer cathode foils of each module serve as gas containment foils as well.

The entire detector assembly, or stack, is placed in a cradle. The stack is comprised of one central target PC module (two planes of target PCs on each side of a target foil in which most of the muons stop) at the stack center, surrounded on each of the upstream and downstream sides by 7 UV pairs of DC modules, 1 DC dense stack (4 UV pairs), and finally at each extremity a PC module of 4 planes. After all modules are arranged into the stack in the cradle, the ceramic glass rings form 4 columns. The columns are compressed (ideally they are in optical contact) over the full length of the stack, so the relative positions and distances between wire planes are well known.

Compression tests have been done to check the total length of the detector. However, pressure applied on the ceramic ring columns deforms the cradle as well. In order to exclude this effect from a measurement of the stack length, the cradle deflection was checked first. The

detector stack was replaced with 4 aluminum cylinders for this measurement and cradle deflection was measured as a function of an applied force. Four dial gauges were mounted on the downstream end of the assembly to measure movements of downstream surfaces of the aluminum cylinders or ceramic glass columns as a function of an applied force.

Another test was done in order to make a direct measurement of the total length of the detector stack when 150 and 300 kg forces were applied to each ceramic ring column. Since there is no access to ceramic ring surfaces when the detector is compressed, four brass fiducial surfaces were installed on the sides of the dense stack gas box ceramic rings at a distance of 2.000 ± 0.005 mm from the ceramic ring faces. The distance between these upstream and downstream brass surfaces was measured using a dial gauge mounted in a holder. Then the dial gauge reading was compared with a measurement of the length of a specially made gauge block of length 1080.030 ± 0.005 mm. Measurement with a 150 kg load resulted in total lengths of ceramic ring columns from the upstream dense stack to downstream dense stack of 1083.751 ± 0.015 mm. The calculated lengths of these columns using measured thicknesses of all ceramic rings gives 1083.787 ± 0.001 mm. The difference is in agreement with the prediction of $24 \mu\text{m}$ compression at 150 kg for ceramic glass with a Young's modulus of 57×10^9 Pa, confirming that the columns are totally compressed. Applying 300 kg force on the ceramic ring columns changed the stack length by a further $27 \mu\text{m}$. Therefore, we know the length of the detector assembly with a precision of about $50 \mu\text{m}$.

The wire positioning on the individual planes (both random positioning errors and wire pitches) and total length of the detector assembly are known with much better precision (at least factor of 10) than required by specification, making any resulting systematic error insignificant. Wire-to-wire alignment within a plane via beam or cosmic ray particles becomes unnecessary due to the high precision positioning of wires.

3.3 Energy loss digitization

All fast readout of the *TWIST* detector system is of time intervals, and takes place via TDCs. In order that energy loss measurements are also possible, a system which converts charge to time intervals has been installed on analogue signals from the target PCs and from the beam scintillator. Each such signal is derived from a split of the preamp or photomultiplier signal (the other part is discriminated for timing purposes) which is routed into what we call a postamp charge to time converter, or PACT. The PACTs were designed around the Lecroy MQT300 chip, which converts charge to a time pulse whose width is proportional to the charge. The result is fed, along with all other timed signals, to Lecroy Fastbus TDCs. Each PACT requires a gate signal, which is derived from the trigger (usually the muon scintillator), so charges from only those signals within 200 ns of the trigger are measured.

TDCs measuring wire hit times in the tracking chambers (DCs and PCs) are operated in the common stop mode, where the interval measured is that between the wire hit and a delayed trigger signal. This is also true of the TDCs reading the trigger scintillator PACT information, while those for the target region PC PACTs use the common start mode. This allows for sparsification that can be set to eliminate the pedestals from the data stream of the target PCs, reducing event size and readout time.

When used on the photomultiplier outputs from the muon trigger scintillator, the charge information allows discrimination between incident muons and positrons. Figure 8 shows the integrated charges of signals from this scintillator; the peak on the right in this figure is produced by the muons (typically ten or more times minimum ionizing) while the peak extending to the threshold at the left hand edge is produced by minimum ionizing beam positrons.

On the target PCs, the analogue PACT information can be used to distinguish muons which stop in the target and to determine the muon stopping distribution. Figure 9 shows the charge distributions for the PCs on either side of the stopping target, in the case of a muon beam whose range is such that most muons stop in the target. In the upper histogram, from PC6 immediately upstream of the target, large energy loss by muons is clearly visible while in the lower histogram,

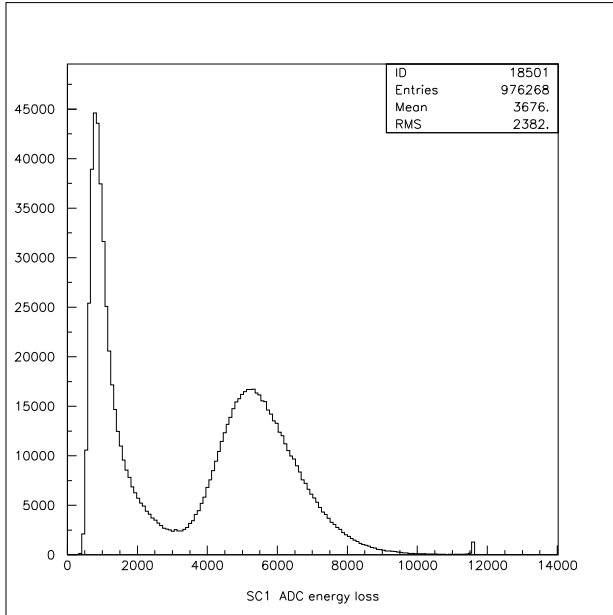


Figure 8: Muon trigger scintillator integrated charge.

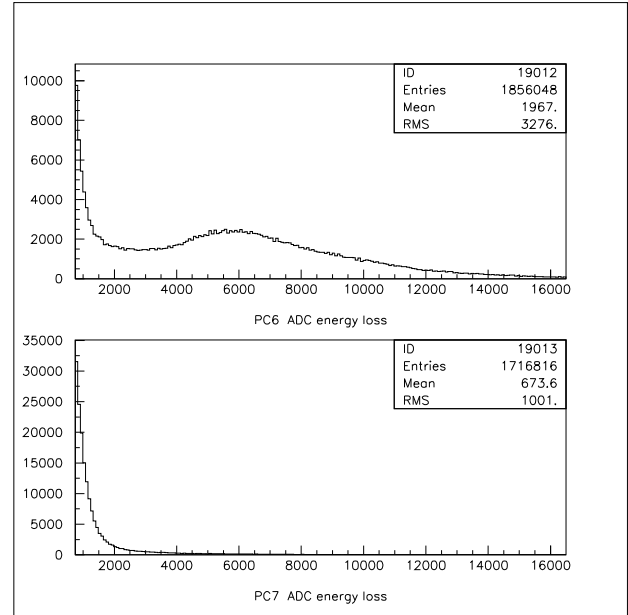


Figure 9: PC6 and PC7 pulse charge distributions.

from PC7 immediately downstream of the target, no muon peak is seen. The analysis algorithm for the target PC PACTs is still being tuned, for example to deal properly with a particle which goes through two cells in a plane where the two energies must be added. Low crosstalk and noise levels in the PCs are important for the analysis to function reliably.

3.4 Time Expansion Chamber (TEC)

At present, muons entering the *TWIST* spectrometer pass through a $3\ \mu\text{m}$ vacuum window, then through a $250\ \mu\text{m}$ plastic scintillator in air, before any position measurement is made by the PCs or DCs of the detector stack. Due to the multiple scattering in these materials, both of which are in the high field region of the spectrometer, the muon tracks do not give information about the path of the particle as it enters the spectrometer field and passes through the region of high radial field components. In fact, because of scattering and also the strong focussing of the solenoid field, we are essentially blind to detailed characteristics of the incident beam.

Because the radial component of the fringe field results in an increase in the divergence of the beam, it also results in an apparent decrease in the average muon polarization (ignoring $g_\mu \neq 2$), since the spin vector follows closely the momentum vector in the magnetic field. The measured value of $\bar{P}_\mu \xi$ is thus sensitive to the distribution in radial positions of the incoming muons where they cross the spectrometer fringe field. The effect is proportional to the magnitude of the radial field which grows with distance from the solenoid axis, so it is therefore important to maintain a minimum beam size at the point where the muons cross the fringe field and to limit the longitudinal extent of the fringe field region. The latter was one of the design criteria for the magnetic return yoke.

To minimize the beam size (and hence the depolarization) by matching the beam parameters to the solenoid fringe field, precise information will be required for the distribution of muon tracks. This in turn will require a very thin tracking detector, since any appreciable multiple scattering in detector materials will make a measurement of the small M13 surface muon beam divergence, $\leq 20\ \text{mrad}$, impossible. For reference, the mean plane scattering angle of a surface muon in a

mylar foil of $6 \mu\text{m}$ thickness is about 5 mrad . We have determined that a low pressure ($\sim 80 \text{ mBar}$) Time Expansion Chamber (TEC) near the entrance to the solenoid is a viable option. A TEC is presently being designed so that it can be installed between the M13 beam line and the solenoid entrance in 2003.

A vacuum box is fitted into the M13 beam tube, into which the TEC can be installed or removed as required. The box, containing the TEC, is positioned between Q7, the last quadrupole of M13, and the CCD alignment system which is upstream of the TWIST magnet yoke, as shown in Fig. 10. Figure 11 shows both the sections of the TEC in its box in the beam line, at a larger scale. The first section will measure x and dx/dz , and the second y and dy/dz .

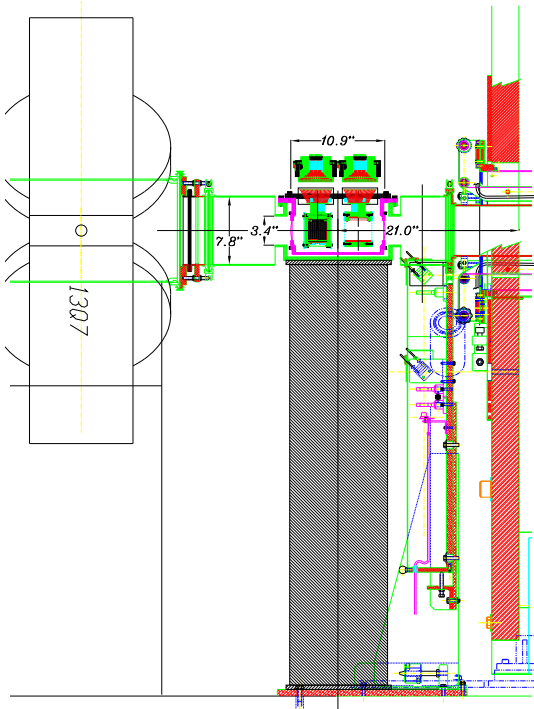


Figure 10: Design drawing of TEC installed between the last quadrupole of M13 and the entrance to the *TWIST* solenoid.

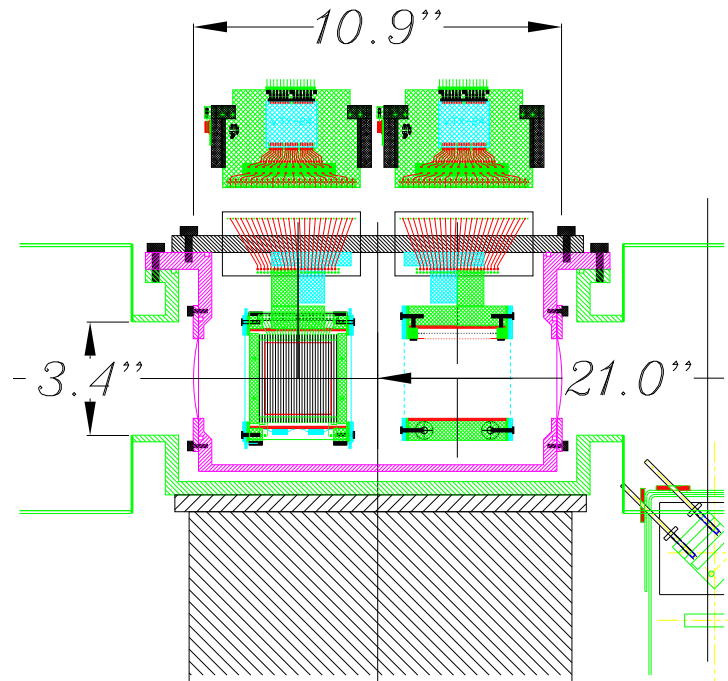


Figure 11: A larger view of the TEC.

Figure 12 shows schematically the section of a TEC that would measure x (the direction to the left of the diagram) and dx/dz ($+z$ is toward the top of the diagram, while $+y$ is out of the page), by drift of ionization perpendicular to the beam direction. It has 48 sense wires indicated by small circles at the left, and a negatively biased plane at the right. Field shaping in this design is via strips on a mylar film at the top and bottom; we are also investigating the alternative of field shaping wires to reduce scattering material in the muon path.

Several of the parameters of the TEC have been determined using GARFIELD and GEANT. A GEANT study has determined that for a TEC positioned as shown in Fig. 10, the drift region, that is the region where there are no materials apart from the chamber gas, must have a transverse dimension of at least 5 cm for passage of an M13 beam which has rms dimension of 10 mm and rms divergence of 30 mrad in x or y . The M13 beam may be tuned for smaller values but the present design, for an opening of 6 cm , will allow an estimate also of the tails of the beam profile.

A study with GARFIELD has shown that the resolution of this chamber will be dependent on the drift distance and thus the position of the hit as shown in Fig. 13. A further GEANT study, including the effects of this resolution function, has shown that a simple straight line fit to

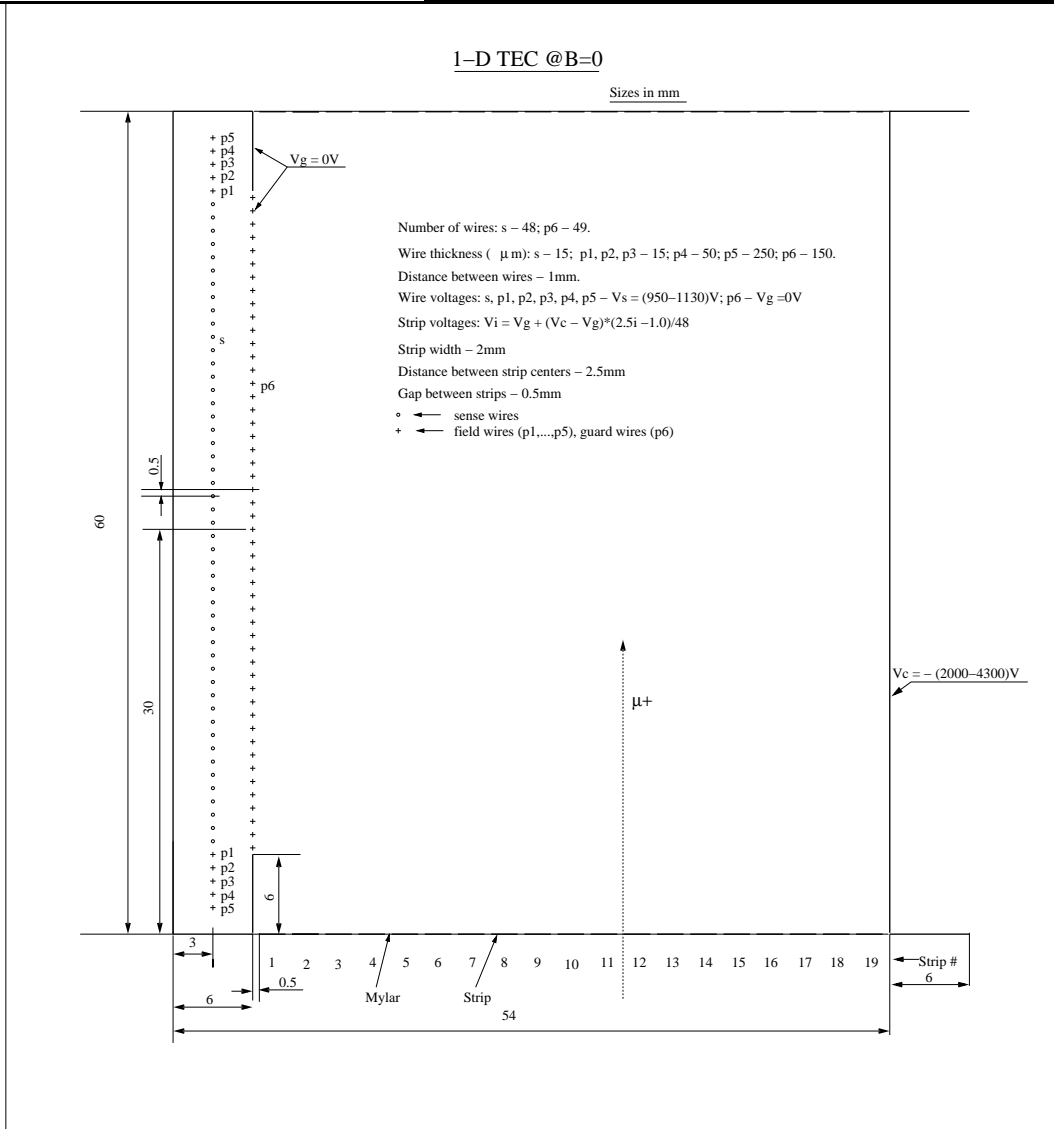


Figure 12: Schematic view of TEC from above.

the hit points is possible if the TEC is positioned sufficiently far from the magnetic field. For the planned position shown in Fig. 10 the standard deviation of fits to a straight line is dominated by the chamber resolution rather than track curvature. The determined values of position x, y and divergence dx, dy were employed to calculate the momentum direction, *i.e.*, the spin, of the muon at the stopping target, which has been shown in our studies to be correlated with the muon spin tracked by GEANT.

Further GEANT studies are presently underway to determine the optimum number of sense wires in each section, the influence of the Lorentz drift angle on the chamber resolution, and whether field shaping is better done with wires or with foils supporting aluminized strips.

4 Systematic Uncertainties

The proposed measurements will be limited in precision by systematic uncertainties in the measurements. For example, statistical precision of ρ to 10^{-4} can be obtained with 6×10^8 events [10], although this assumes use of the full positron energy range and is therefore somewhat low.

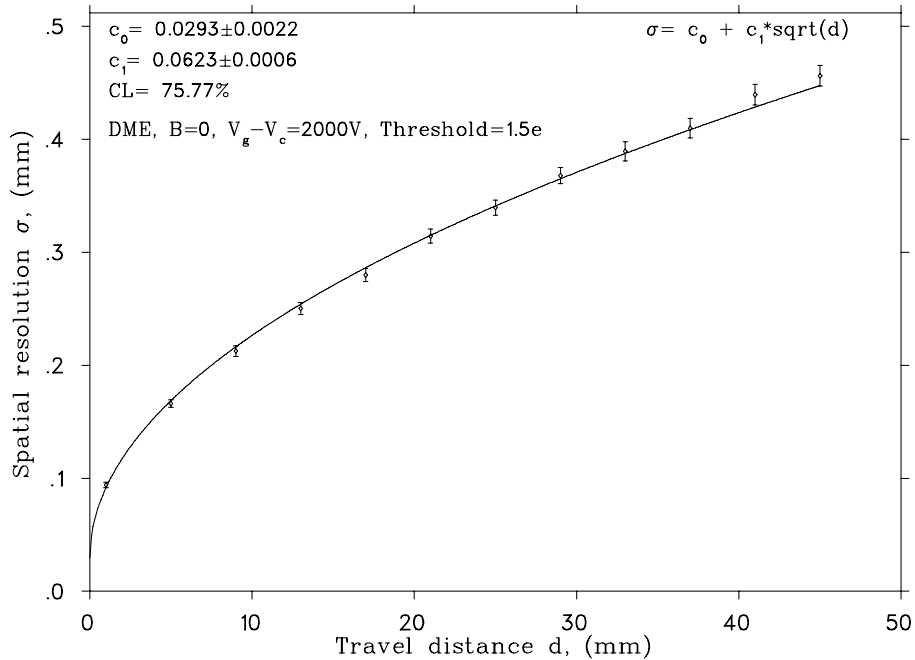


Figure 13: Resolution of TEC vs distance.

At the present data acquisition rates (1000 reconstructable events per second), this takes less than 200 hours; we hope to improve the rates in the near future. The important point is that systematic tests will take much longer.

An advantage in *TWIST* is that because nearly the entire decay spectrum is measured the data are simultaneously sensitive to all four of the Michel parameters. This allows for a reduction in the combined systematic uncertainty. The previous measurement of δ had a significant uncertainty (1 part per 1000) due to the precision of previous measurements of ρ (4 parts per 1000). The *TWIST* collaboration will not only be able to determine all four Michel parameters, but will also be able to produce complementary data sets with correlations differing from those in Table 4, thus reducing corresponding uncertainties and increasing our sensitivity to the physics parameters.

	ρ	δ	η	ξ
ρ	1	0.22	0.97	0.83
δ		1	0.18	-0.29
η			1	0.83
ξ				1

Table 4: Correlations between the Michel parameters in the raw μ decay spectrum. The *TWIST* spectrometer allows for the production of data samples with differing correlations.

For example, the data set

$$N_+ = N_{upstream} + N_{downstream} \quad (4)$$

is sensitive to ρ and to η , but is insensitive to δ , ξ , or to the muon beam polarization. Similarly, the data set

$$N_- = N_{upstream} - N_{downstream} \quad (5)$$

is sensitive only to δ and $P_\mu\xi$.

In addition, it will be possible to obtain an unpolarized beam with a polarization of 0.00 ± 0.05 . This will allow us to make a largely independent measurement sensitive primarily to ρ and to η . It is important to stress that the use of multiple data sets with differing sensitivities provides consistency checks which enhance the strength of the final result.

The detector design is predicated on the requirements that:

1. The energy scale of the spectrum must be determined to better than one per 10^4 .
 - It is important to note that the system is designed with a high degree of linearity. It is the geometry of the detector, along with the uniform magnetic field, that defines the energy scale.
 - The system has been designed to have very little mass. For comparison, a previous experiment was done with 240 to $270 \text{ mg} \cdot \text{cm}^{-2}$ in the path of the decay positrons[11, 12]. The *TWIST* spectrometer is produced with a total of $15 \text{ mg} \cdot \text{cm}^{-2}$ in the path of the decay positrons prior the tracking volume.
 - Important design considerations include the use of planar chambers, for which the energy loss is particularly simple. In particular,

$$\frac{dE}{dz} = \frac{dE(\cos(\theta) = 1)}{dz} \cdot \frac{1}{\cos(\theta)} \quad (6)$$

This means that average corrections for energy loss are rigorous and straightforward.

- Because the detector views the entire spectrum in a single bite, the energy scale is calibrated by the end point of the Michel spectrum itself. External calibrations are not required.
2. The absolute angular scale of the spectrum must be determined such that the apparent depolarization magnitude ($1 - \cos^2 \theta$) is known better than one in 10^4 , setting a limit of about 14 mrad. However, stringent requirements must be met within the detector, by knowledge of wire geometry, to avoid systematic distortions of the Michel spectrum shape.

Many of the systematic effects trace to these requirements. Contributions to the total systematic uncertainty are summarized in the list of Table 5. Below are descriptions of the entries in the table, numbered for convenience.

- 1 The transverse distance scale and the magnitude of the magnetic field together set the energy scale. It is a significant feature of the experiment that the large acceptance of the device allows the energy scale to be calibrated by the endpoint of the Michel spectrum without the adjustment of either angles or fields. We have shown that we can produce a beam with a polarization of 0.00 ± 0.05 with a flux of $\sim 200 \text{ Hz}$ by making an appropriate timing cut which mixes surface and cloud muons. The spectrum produced by this beam has an isotropic decay distribution, so that the energy calibration can be done for all angles throughout the spectrometer by studying the endpoint of the energy spectrum at 52 MeV.

In this way, we can determine the endpoint of the Michel spectrum to about 4 keV. Since the field is constant and the wires are uniformly spaced the system is linear and the endpoint determines the energy calibration. Nonetheless, a means of verifying the calibration from the Michel spectrum exists by looking at the shape of the distribution at $x = 0.5$ and at $x = 0.75$:

$$M = \frac{\frac{\delta}{\delta x}(d^2N(x = 0.5, P_\mu = 0)/dx d\cos(\theta))}{(d^2N(x = 0.75, P_\mu = 0)/dx d\cos(\theta))} = \frac{16}{9}. \quad (7)$$

While we expect to be able to calibrate the system to considerably less than 10 keV, this conservative assumption was made in determining the associated uncertainties in the Michel parameters shown in the table.

##	Source of Correction or/and Error	$(1 - P_{\mu}\xi)$ (10^{-5})	$(0.75 - \rho)$ (10^{-5})	$(0.75 - \delta)$ (10^{-5})
1	Positron energy calibration	± 3	± 5	± 5
2	Intrinsic DC resolution	< 1	< 1	< 1
3	Deviation of average distances in DCs assembly	± 0.75	± 1.2	± 1.2
4	Random errors (20 μm) in sense wire positions	$\ll 1$	$\ll 1$	$\ll 1$
5	Wire sags ($< 1 \mu\text{m}$) in DCs	< 1	< 1	< 1
6	DCs' misalignment ($< 1 \text{ mrad}$) with respect to B direction	< 1	< 1	< 1
7	Magnetic field inhomogeneity ($< 10^{-4}$)	$\ll 1$	$\ll 1$	$\ll 1$
8	Beam flux ratio $e^+/\mu^+ = 4$	$\ll 1$	$\ll 1$	$\ll 1$
9	Muon decay in flight	$\ll 1$	$\ll 1$	$\ll 1$
10	Deviations of temperature (1°C), pressure ($3 \cdot 10^{-3}$), H.V. ($3 \cdot 10^{-3}$) in DCs	$\ll 1$	$\ll 1$	$\ll 1$
11	Tracking time-zero	$\ll 1$	$\ll 1$	$\ll 1$
12	Lorentz drift angle ($< 8^\circ$) in DME gas at 2 T	< 1	< 1	< 1
13	Non-uniformity of detector acceptance	< 1	< 1	< 1
14	Corrections to the response function	± 6	± 5	± 5
15	Coulomb scattering of muons inside the production target	± 1	-	-
16	Non-surface muon contamination	± 3	-	-
17	Fringe field depolarization of muon	± 3	-	-
18	Instability (10^{-4}) of current in M13 bending magnets	± 3	-	-
19	Proton beam shift ($\pm 0.5 \text{ mm}$) on the production target	± 4	-	-
20	Misalignment ($< 0.1 \text{ mrad}$) of B with respect to the beam direction	< 1	-	-
21	Depolarization of thermal muon in metal at 2 T	< 1	-	-
22	Muon depolarization due to muon stops in last PC	± 2	-	-
23	Creation of thin ($\ll 20 \text{ \AA}$) films on the surface of the stopped Al target	$\ll 1$	-	-
24	Muon scattering by unpolarized electrons	± 0.5	-	-
	Anticipated systematic uncertainty	± 10	± 7	± 7
	Statistical errors for 10^9 events	± 10	± 5	± 8
	Anticipated uncertainty	± 14	± 9	± 11

Table 5: Sources of systematic uncertainty.

- 2 A wire chamber resolution of $100 \mu\text{m}$ has been shown to result in an angular resolution of $< 7 \text{ mrad}$ over most of the spectrometer acceptance. This smearing has a negligible effect on the extracted Michel parameters.
- 3 The individual wires were mapped during assembly (see section 3.2), and wires deviating by more than 20 microns from their intended position were restrung. The measured positions of the wires in one typical plane are shown in Fig. 14. The variation in the deviation of wire positions from their nominal value has an average which is much less than $0.1 \mu\text{m}$. This introduces an error of 0.1 in 320,000 in the measurement of angles, which has a negligible effect on the extraction of the Michel parameters.

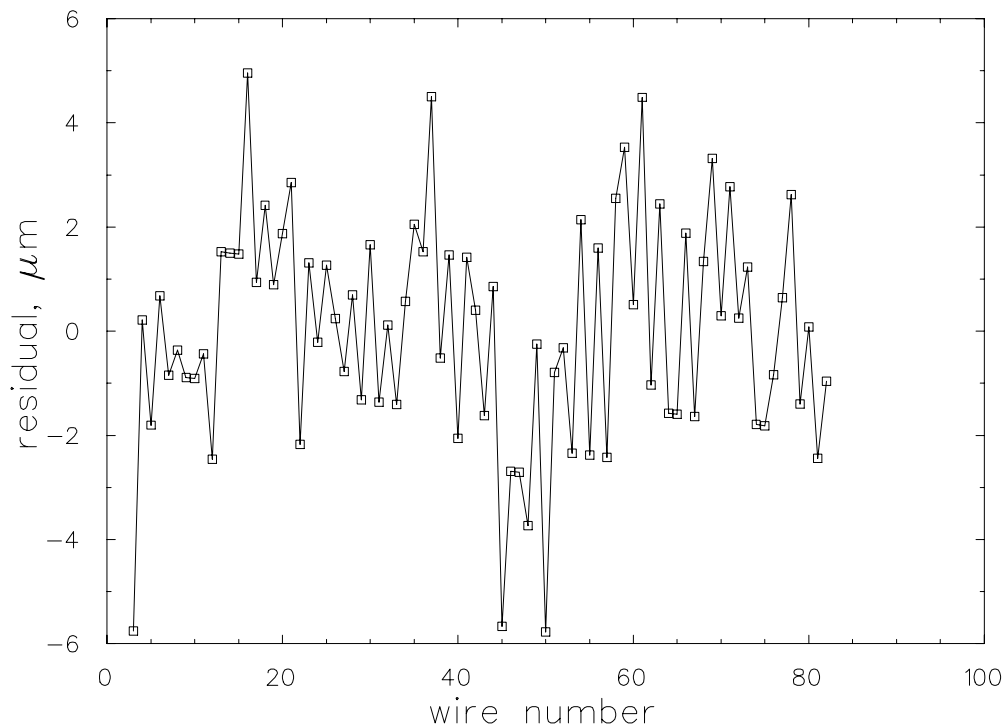


Figure 14: Each wire position was measured with a precision microscope during assembly. Outlying wires were replaced. A typical scan of a wire plane in X is shown above. Wire positions are correct to within a standard deviation of $3 \mu\text{m}$. In the final analyses these mapped wire positions will be used in the track reconstruction.

The length of the stack is determined by four columns of ceramic citals. Each cital has been measured to a precision of $0.5 \mu\text{m}$. The total length of the stack was measured after compression of the citals, confirming a measurement precision of better than $50 \mu\text{m}$ which corresponds to a systematic uncertainty of $0.5 \cdot 10^{-4}$ in the determination of angles. This introduces very small uncertainties in to extracted Michel parameters.

- 4 The effect of random errors of wire positions on the Michel spectrum is negligible. Simulations show that for $\sigma \leq 20 \mu\text{m}$ the resulting shift in the derived momentum is $|\Delta p| < 1 \text{ keV}/c$ and in the measured angle $|\Delta\theta| < 2 \cdot 10^{-6}$. These effects have negligible effect on the extracted Michel parameters. In reality, the as-built chambers exceed this condition by a factor of ~ 7 . The standard deviation of the wire positions shown in Fig. 14 is $\sim 3 \mu\text{m}$. The deviations from the mapped positions is smaller still.

- 5 The wires are (W-Re)Au with a diameter of $15 \mu\text{m}$ and a length of 40 cm stretched with a force of 30 g. Maximal gravitational sag of a wire is about $1.3 \mu\text{m}$ at the center of a horizontally stretched wire.
The *TWIST* wires, however, are stretched at 45° , so their gravitational sag is approximately $1 \mu\text{m}$ at the center. The reconstructed helix is maximally distorted for events which hit near the end of the wire, then near the middle, and again near the end. For wires of length ~ 40 cm and planes separated by 40cm at minimum, the maximal distortion is the order of $2 \cdot 10^{-5}$ which causes negligible distortion to the angles or the energy scale, and therefore negligible perturbation to the extracted Michel parameters.
- 6 Any unknown misalignment of the detector stack with respect to the magnetic field axis will result in an error in the angle scale. Therefore, the orientation of the stack with respect to the field must be known to 14 mrad in order to maintain a depolarization of less than 1 in 10^4 . The misalignment will be measured by looking for a systematic bias or ϕ dependence in the axis of helices. In principle, this can be removed by adjusting the physical orientation of the chambers, but in practice a calibration constant may be applied.
- 7 Uncertainty in the field uniformity at one part in 10^4 has a small impact on the energy scale. We now map to this precision, and will improve this precision in a future field map, including the fringe field region which is important for item 17. The actual magnitude of the magnetic field is calibrated by determination of the energy scale.
- 8 The positron flux exceeds the surface muon flux by approximately a factor of 4. Running with a muon flux of 5 kHz and a decay timing gate of $10 \mu\text{s}$, roughly 20 percent of events will include a beam positron. Roughly 10% percent of these events will see a beam positron in time with the decay positron, and roughly 2% of these events will contain a positron which will pose tracking uncertainty due to a spatial confusion of hits. In summary, roughly 4 in 10^4 of the muon decay events will contain a beam positron which creates tracking ambiguity. This will have a negligible effect on the angular distribution.
- 9 The influence of the decay of muons in flight has negligible influence on the Michel spectrum. Prompt muon decays are cut from the analyzed data sample, and this cut will also remove muon decays in flight.
- 10 Calculations of drift properties have been made using Garfield [13]. These estimates have been compared with measured properties, and have been found to be a reliable estimate of chamber performance. The sensitivity of these calculations to drift chamber operating parameters (temperature, pressure, and high voltage) has been checked over the conservative ranges indicated.
- 11 The set of PCs provide a timing accuracy of ~ 2.5 ns. This would result in a 25 micron contribution to the tracking resolution. The final tracking, however, will combine the PC timing with the overall tracking fit with t_0 determined as a parameter of the fit. This results in a timing resolution significantly better than 2.5 ns. At an average drift speed of $10 \mu\text{m}/\text{ns}$, this results in a negligible systematic uncertainty in the Michel parameters.
- 12 The small value of Lorentz drift angle ($\theta \leq 8^\circ$) was one of the arguments in favour of choosing DME gas for E614 spectrometer. The small angle results in small corrections due to the effect of the magnetic field on charge drifting in the DCs. This results in effective drift distances which are increased by at most approximately $24 \mu\text{m}$. This is readily corrected in the tracking, and results in a negligible effect on the extracted Michel parameters.
- 13 The efficiency of the *TWIST* drift chambers has been measured, and has been found to exceed 99.5%. The probability of missing three chambers is therefore $\sim 10^{-7}$. Because the system comprises 22 DCs in each half stack, and because most helical tracks trigger wires

in more than one cell per plane, the system is highly redundant so the probability of having insufficient hits for the tracking reconstruction is negligible.

For various reasons, the efficiency may be reduced by individual wires which are either dead or are producing insufficient output. The wires near the target are optimal for track reconstruction, as energy loss and multiple scattering have had less impact upon the decay distribution. Therefore, suppose we consider tracking using only the first 12 DC planes. In this case, the helix is overdetermined and the fit typically has at least 6 degrees of freedom (assuming only one hit per plane - in reality most helical paths produce multiple hits per plane). If we allow one dead wire in each plane, the probability of a track involving only one dead cell is

$$P = \left[\frac{1}{80}\right] \cdot \left[\frac{79}{80}\right]^{11} \cdot \frac{12!}{1!11!} = 13\%. \quad (8)$$

A difficulty occurs when the number of degrees of freedom in a given track is compromised. Given 12 DC planes there are six degrees of freedom. Consider the case of four dead cells along a track, leaving only two degrees of freedom. If one cell is dead in every plane,

$$P = \left[\frac{1}{80}\right]^4 \cdot \left[\frac{79}{80}\right]^8 \cdot \frac{12!}{4!8!} = 1.1 \cdot 10^{-5}. \quad (9)$$

For the case in which every plane has two wires which are dead, the probability of losing four planes becomes

$$P = \left[\frac{2}{80}\right]^4 \cdot \left[\frac{78}{80}\right]^8 \cdot \frac{12!}{4!8!} = 1.6 \cdot 10^{-4}, \quad (10)$$

by which point the potential effect upon the distribution becomes significant.

We will generally require that dead wires be limited to no more than one per plane. All wires are not, however, of equal importance. We may require, for example, that all wires near the target and near the axis be working properly.

It is more likely that a positron helix may pass through a portion of the chamber which has been disabled by space charge effects. It is estimated that approximately 1 mm along a wire will be dead for several microseconds after the passage of an incoming muon [14]. This has a significant effect on the detection of positrons which spiral back along the path of the incoming muon. This effect is reduced considerably by energy loss which decreases the radius of the helical path, and by multiple scattering which alters the positron trajectory.

It is estimated that the probability of passing through one space-charge affected zone in 12 DC planes is approximately 3%, two space-charge affected zones (or more) is 0.3%, three space-charge affected zones (or more) is 0.04%, and four or more space-charge affected zones is 0.02%. As the positron moves deeper into the stack, the decay of the spiral actually takes it further from the incident muon trajectory. Note that energy loss in the system is 7 keV/module/cos(θ) (here module refers to a pair of *UV* planes). This decreases the radius of curvature by approximately 0.1%/cos(θ) per module, or roughly 100 $\mu\text{m}/\cos(\theta)$ per module.

14 The positron energy loss over the length of the *TWIST* detector is given by

$$\Delta E(\theta) = \Delta E(\theta = 0) / \cos \theta \equiv (\alpha + \beta E) / \cos \theta$$

where θ is the polar angle with respect to magnetic field, E is the positron energy, and α and β account for the energy dependence of the energy loss. The latter linear function is a very good approximation for the energy losses of positrons in the range $E = 20 - 60$ MeV (see data in [15]). A Monte Carlo study of the energy loss versus $1/\cos(\theta)$ has shown that the detector does in fact follow this dependence very accurately, indicating that an

energy calibration of the detector to better than 4 keV will be possible. In this study β was taken to be zero and α was treated as a free parameter. The accuracy to which one can extract the energy spectrum, and hence the Michel parameters, is defined by the uncertainties of energy losses of positrons in matter. These have been estimated to be 1 to 2 percent [16]. Conservatively assuming that these uncertainties are at the 4% level the uncertainty in the derived Michel parameters will be $\sigma(\rho) = \pm 5 \cdot 10^{-5}$, $\sigma(\eta) = \pm 4 \cdot 10^{-3}$, $\sigma(P_\mu \xi) = \pm 6 \cdot 10^{-5}$, $\sigma(\delta) = \pm 5 \cdot 10^{-5}$. It must be noted that in fact it may be possible to do much better than this using modern knowledge of the positron energy loss in materials. For example the GEANT4 collaboration is incorporating information gleaned from micro dosimetry studies.

- 15 Coulomb scattering breaks the correlation between the momentum and spin directions. If this takes place before the momentum direction is determined, then there is no handle on the spin direction. This is not an issue in the final stopping target, since the initial momentum vector has been determined by beam transport into the spectrometer system. However, a muon may scatter in the graphite production target, following decay of a pion occurring at non-negligible depth below the surface of the target. In this case, the direction in which the muon exits the target into the M13 beam transport system is not exactly the initial momentum direction, resulting in some amount of depolarization. This can be controlled by precise momentum selection of only the most energetic surface muons, which originate closest to the surface and undergo the least amount of Coulomb scattering. The effect is shown in Fig. 15 which shows the depolarization due to Coulomb scattering as a function of the depth at which the pion decays to produce the muon. The momentum acceptance ($\frac{\Delta p}{p} = 1\%$) of the channel is such that we can limit the data sets to muons produced within about 25 μm of the surface, so that corrections due to Coulomb scattering are small.

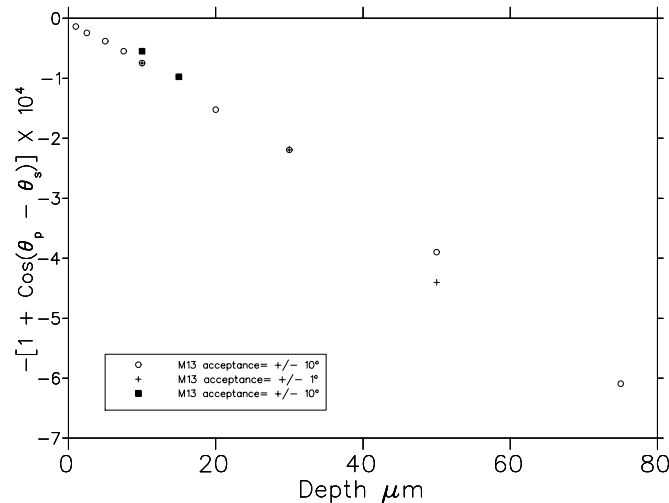


Figure 15: Muon “depolarization” in the 1AT1 Target. Here θ_p and θ_s are the final and initial momentum directions respectively. The hollow circles and crosses are the results when no momentum selection was made on the outgoing muon. The filled squares are the results when the outgoing momentum of the muon was restricted.

- 16 The polarization of the background and background flux has been measured at M13. This was done by adjusting the momentum just above the kinematic limit for the decay of pions at rest to muons. The cloud muon flux has been found to be 3% as great as the surface muon flux, and to have a polarization of 0.3 (oriented opposite that of the surface muon

polarization). The cloud muons are readily cut from the data by their time of flight relative to the cyclotron bunch time. The surface muon flux, the estimate background, and the muon asymmetry are shown as a function of the cyclotron timing in Fig. 16.

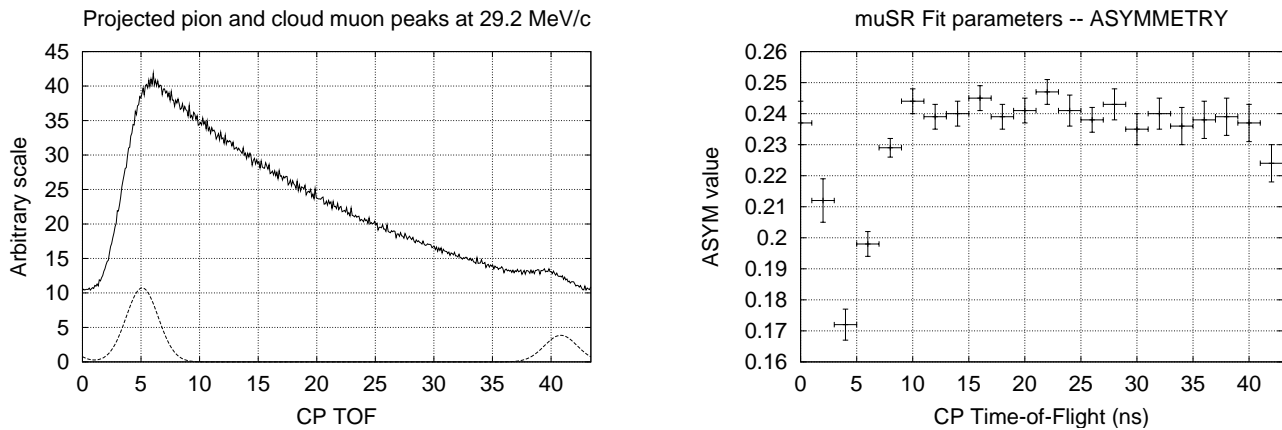


Figure 16: The upper curve in the figure at the left is the time-of-flight of surface muons. The distribution is characteristic of the π^+ half life, since the pions are at rest on the surface of the production target when they decay. The lower curve at the left is the distribution of background particles, measured at slightly higher momentum and extrapolated to the momentum of the surface muons. Muons are visible near 5 ns in the figure, and pions near 42 ns. Both of these contaminants can be removed by the use of a timing cut. The figure at the right shows the polarization asymmetry measured across the the same cyclotron timing window.

There are also muons above the surface muon momentum which are not correlated with the cyclotron bunch time. The polarization of these muons has been measured, and it is found that these muons are actually the tail of the surface muon momentum.

The effect of non-surface muons is negligible.

- 17 A second example of apparent depolarization has been identified, and will take substantial effort to assess experimentally. It is due to the extra beam divergence introduced by radial magnetic field components as muons pass through the fringe field of the solenoid. Minimization of this source of depolarization requires careful matching of beam parameters to the solenoid fringe field. Essentially this means that the beam size should be as small as possible in the fringe field region, as the radial components farther from the beam and solenoid axes are greater. As well, the magnetic return yoke has been designed to limit the spatial extent of the radial fringe field.

The effect enters as the cosine of the angle of the spin with respect to the field axis as the muon stops in the stopping target. The effect of particles crossing the fringe field off axis, or at an angle to the axis is shown in Fig. 17. A final angle of 14 mrad corresponds to an apparent depolarization of 10^{-4} .

We will use a very low mass Time Expansion Chamber (TEC; see section 3.4) to measure and adjust the beam profile at the entrance to the spectrometer. The final data set for $P_\mu \xi$ may be taken with a limited emittance beam at reduced rate. The anticipated beam flux as a function of the stopped muon orientation is shown in Fig. 18.

- 18 Any instability in the bending magnets of the beam line can affect the muon polarization. First, since they select the beam momentum, a variation of both bending magnets either up or down will lead to muons in the *TWIST* spectrometer which are produced at a different depth in the target. They will therefore have a different average degree of depolarization, as described in the item on Coulomb scattering.

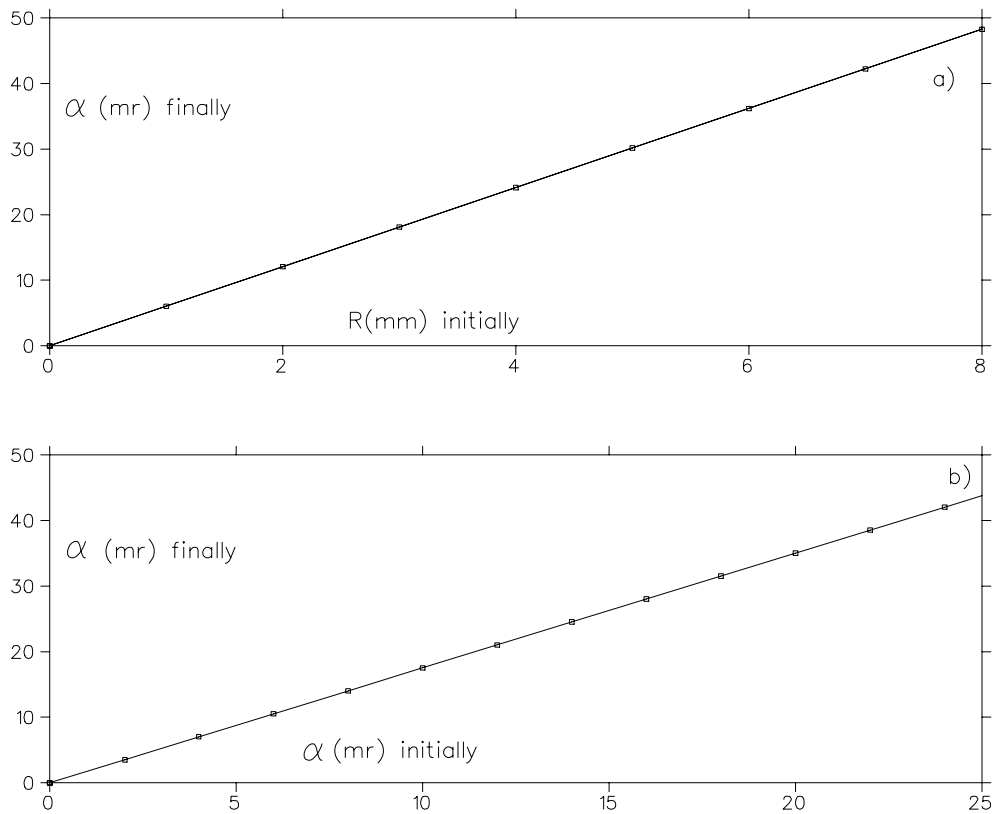


Figure 17: The effect of the radial position of the muon as it crosses the fringe field (a) and the effect of the incident muon angle (b) on the angle of the muon spin as it stops in the target.

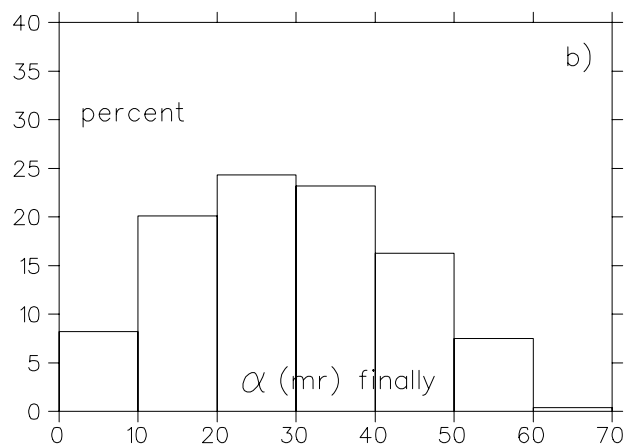


Figure 18: The relative beam flux as a function of the stopping angle of the spin relative to the field axis.

Second, if one or the other of the magnets changes, the mean horizontal beam position is changed. Since depolarization of the muon as it passes through the fringe field region of the *TWIST* spectrometer depends on the distance of the muon path from the (zero radial field) spectrometer axis, the average depolarization is changed as discussed in the item on fringe field depolarization.

The stability of the currents of the bending magnets has been verified to substantially exceed our stated requirements of one part in 10^4 for B1. The second bending magnet, B2, is not as good, but we expect to be able to achieve a similar specification. NMR probes are installed which allow monitoring of the fields to this precision; they have recently been included in the bending magnet control feedback loop.

A part in 10^4 variation in the dipole fields results in a depolarization due to Coulomb scattering 100 times smaller than the range of the momentum acceptance. This has a negligible effect on the polarization.

The effect of the variation in steering across the fringe field will require extensive study.

- 19 A variation in the proton beam position causes a variation in the position of the image of the source at the entrance to the *TWIST* spectrometer. Therefore, the movement of the proton beam leads to variations in the effective polarization similar to the effects of dipole steering.

A vertical displacement of the proton beam on the 1AT1 target of 0.5 mm will result in a change in the muon beam direction at the entrance to the spectrometer of $\Delta\theta = 0.5$ mrad. This directly corresponds to a $(1 - P_\mu\xi)$ shift of $3 \cdot 10^{-6}$. It also leads to a 0.75 mm transverse displacement of the muon beam in the fringe field area at the entrance to the solenoid, which contributes 4×10^{-5} to the systematic uncertainty in the beam polarization.

- 20 The misalignment of the magnetic field \vec{B} with respect to the direction of P_μ will result in an effective decrease in the muon polarization. The alignment can be determined by use of an auxiliary detector which will use traditional μ SR in the solenoidal field to look for the precession of transverse components of the muon polarization.
- 21 All possible mechanisms of muon depolarization in an Al stopping target lead to depolarizations that are very small at $B = 2$ T if the admixture of ferromagnetic elements (Fe, Co, Ni) in Al is less than 10 ppm. High purity Al will be used for one of the targets, and comparison will be made with others such as high purity Ag, via a target module with selectable target materials.
- 22 A Monte Carlo study of the stopping distribution of muons in the stopping target and in the neighboring PC detectors has shown that pulse height information from these detectors can aid substantially in rejecting those muons that have not stopped in the target. For this purpose the signals from these detectors has been divided so that such pulse height information should be available. In addition this study showed that the ratio of hits in the PCs upstream of the stopping target to those downstream change significantly if the stopping distribution becomes skewed in either direction. This fact will provide a monitor of the stopping distribution.

Those muons that stop in the detector components may suffer depolarization so eliminating them from the sample is important for the $P_\mu\xi$ determination. The target for the initial stages will be a mylar foil which will allow a determination of the depolarization factor for the foils of the PCs. From the MC study the fraction of muons that stop in the gas of the PCs was found to be 9.7%; cuts based upon the PC pulse heights reduce this sample to 0.8%. The depolarization of muons stopped in the PC gas has been measured ($P_\mu = 0.985$) so the resulting correction to the final P_μ of 1.2×10^{-4} .

Personal Identification No. (PIN) 49910	Family Name of Applicant MARSHALL
---	---

In a 10^9 target stopped muon sample a further $\approx 4 \times 10^{-7}$ will be positively identified as having stopped in the PC gas by the signal they give in the upstream/downstream PC before appearing as a track in the downstream/upstream half of the detector. These muons that are identified as having stopped in the PC gas will be used to determine these factors to high accuracy, keeping the error on this correction small.

23 Muon depolarization is possible in solid films which can be formed on the surface of the stopping target. In [17] the thickness of solid film on the surface of PC anode wire was measured after an accumulated charge ≈ 5 C/cm which corresponds to more than 10^{12} detected particles per cm of sense wire. The mixture CF_4/Iso (80/20) was used as a drift gas. Thickness of the film was found to be 20 Å, primarily carbon.

At the same time, an attempt was made to study deposition on a pure Al film. Estimates based upon Auger spectroscopy are that these films are very thin. It is expected that a negligible fraction of the stopping muons will stop in these surface layers.

24 Depolarization of muon when slowing from $p = 29.8$ MeV/c down to zero is calculated in [7][8][18]. The effect is negligible if the incident muon has a kinetic energy of at least ~ 200 keV when it enters the solid target.

5 Status and Recent Developments

TWIST first used the muon beam into a partially instrumented spectrometer in 2001. During some of that time, almost all of the detector stack was operational, although the PACT system had not been commissioned. In early 2002, the first detailed field map was obtained with the radial volume mapping system (see section 3.1).

Following that, in preparation for scheduled beam operation in the summer of 2002, we encountered a problem with the solenoid. A vacuum leak had occurred, and air had entered the solenoid vacuum chamber where it cryopumped to the cold interior surfaces. On energizing the solenoid, it quenched. Due to loss of cryogenics, the temperature rose enough that the cryopumped air was released, and we had no choice but to warm the solenoid.

The cost of this quench was significant in terms of time, money, and human resources. We were not able obtain operating temperature of the solenoid until late August, and managed to use only a fraction of the summer's allocated beam with the field on. On the other hand, we believe that the experience gained will allow us both to avoid a possible quench in future and to recover from a warmup more quickly and efficiently. We also used the time to learn as much as possible about the detectors and the beam as was possible without the solenoid field.

At the time of submission of this proposal, we anticipate over two months of running time in the fall of 2002. At the same time, we have begun to study in detail the data that we have so far obtained, to ensure that the data we do take will provide us not only with first measurements of ρ and δ , but also with a better understanding of our systematic uncertainties for all parameters of the positron spectrum. Some of these very preliminary results are presented in the remainder of this section.

5.1 Chamber calibrations

In the past year a detailed study of the chamber performance was conducted including chamber efficiency, noise, cross talk, and resolution. The efficiency of both the drift and proportional chambers was studied in detail at various high voltages and thresholds. The efficiency curves as a function of high voltage were calculated for each of the 44 DC planes and each of the 12 PC planes. In addition, efficiencies for every DC and PC wire were calculated to confirm that no significant variations are seen across a plane. The DC planes efficiency was found to be above 99.9% for all 44 planes with plane to plane variations below 0.04% as may be seen from Figure

19. Figure 20 shows the efficiency as a function of high voltage for DC plane 1, which is typical of all other DC planes. The PC plane efficiencies were found to be around 99.9% with plane to plane variations being less than 0.07%.

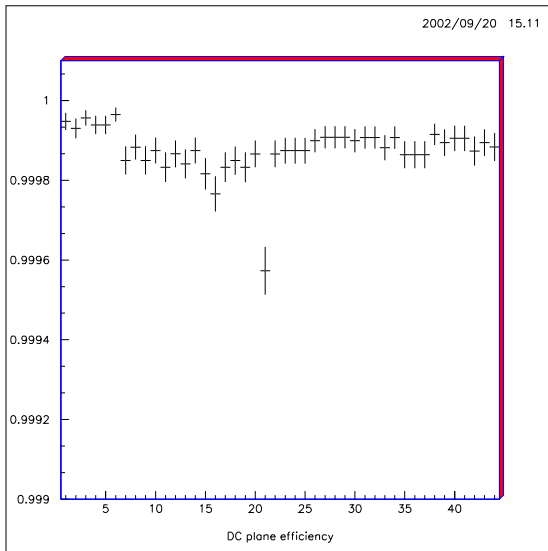


Figure 19: Efficiency for the 44 DC planes at the operating high voltage and threshold.

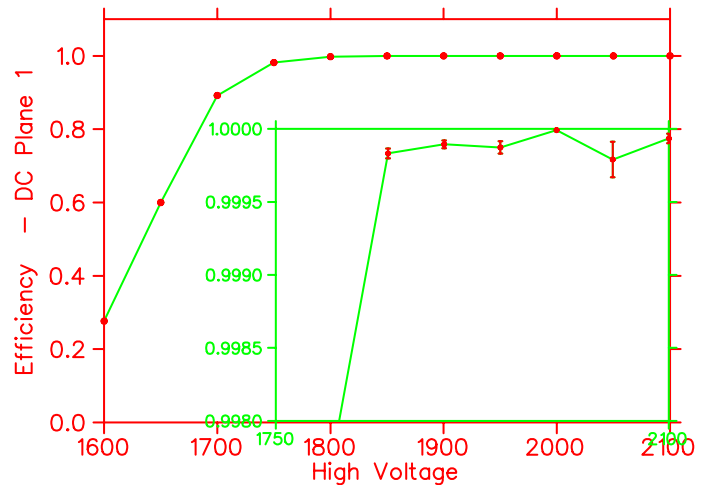


Figure 20: Efficiency of DC plane 1 as a function of high voltage at the operating threshold.

The efficiency code was subjected to rigorous tests to detect possible biases. Hits were randomly rejected with various percentages right after the data unpacking, and the efficiency was calculated. The efficiency code was shown to detect a hit rejection factor as small as 0.1%, confirming that the efficiency calculation is accurate at least to this level.

The noise and cross talk levels were also closely examined. Noise and cross talk levels were calculated at the various high voltages and thresholds for every DC and every PC plane. It was found that in the DC, cross talk signals have a short TDC width making them easy to identify. Combining this cross talk feature with the requirement that a cross talk signal should be within few cells from a real signal (one with a long TDC width) and should coincide in time with a real hit, cross talk hits can easily be identified and eliminated in the software.

This criteria also works for PCs, however, since PC drift times are much shorter than those of the DC, the time coincidence requirement between a cross talk signal and a real signal is not effective. The PCs, however, are not used for tracking, and eliminating PC cross talk hits is therefore not critical. One exception is the target PCs where ADC information is used to determine whether the muon stopped in the target or in one of the neighboring PCs. If cross talk hits are assumed to be real hits, the total energy deposited in the target PCs will be overestimated. The issue of how to use the PCs in the best possible way to identify muon stop positions is still under investigation, and their operating point have not yet been determined pending the completion of these studies.

The noise level in both the DC and PC planes was found to be negligible at the operating thresholds, even when the high voltage corresponded to a point at the high end of the efficiency plateau.

A detailed study of chamber calibrations has also been conducted including time zero determination and plane alignments. The determination of the synchronicity of signals from all the DC and PC wires was made from runs with the solenoid field off, using 120 MeV/c pions defocused to illuminate all wires in the chamber, and a trigger given by a scintillator placed at

the exit of the stack, beyond the magnet yoke. Time of flight of the pions through the chambers was accounted for. The time spectrum for each wire in the prompt region was fit with an error function rise multiplied by an exponential fall off beginning near the maximum of the time spectrum. Fits with very reasonable χ^2 distributions are obtained using this shape. Figure 21 shows sample plots taken with the standard trigger incident particle trigger, with solenoid field on. The fits are overlaid on data for the central wires of DC plane 21. The timing position determined for each wire, defined as the value halfway up the error function rise, is determined to an accuracy of ~ 1 ns. At this level, time zero uncertainties are not expected to affect the position resolution of the spectrometer.

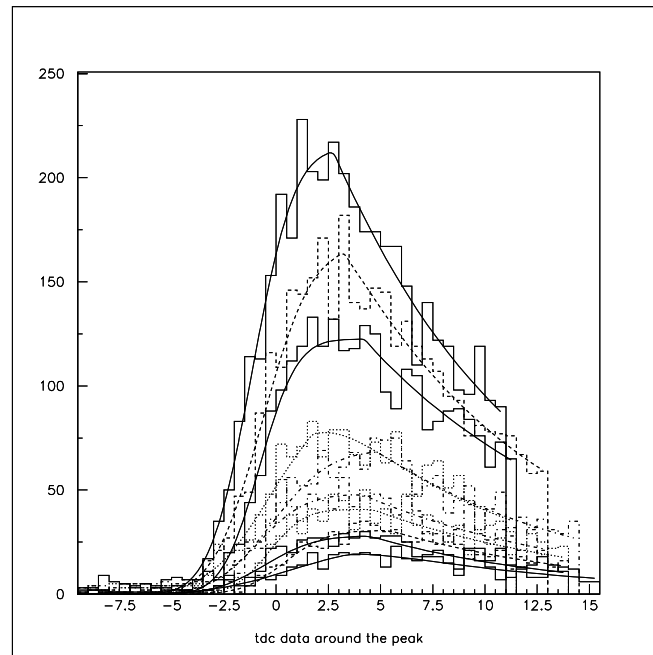


Figure 21: Sample fits to the TDC spectra used to obtain time zero for several wires in DC plane 21.

Plane position corrections were calculated independently by two groups (two different codes) and the results were compared for consistency. The high resolution of the DCs allows accurate plane position alignments which will allow accuracies at the few micron level. However, since chamber calibrations (time zero, resolutions, etc) are interdependent, iterations between these various processes will be required to achieve such a high accuracy. Figure 22 shows the residuals calculated from a Kalman filtering process before plane position corrections were determined. Only approximate timing information was used to produce this plot. These data were taken with the field off using a 120 MeV/c pion beam. Figure 23 shows the residuals as a function of plane number from the same analysis for the 22 upstream DC planes. Misalignments of up to $\sim 300 \mu\text{m}$ can be seen from this plot. Figure 24 shows the same residuals after plane position corrections are incorporated and drift timing information is used. A significant improvement is readily seen bringing the half width of the residuals distributions from $\sim 600 \mu\text{m}$ microns to ~ 85 microns. Figure 25 shows the residuals *vs* plane number for the 22 upstream DC planes.

Figure 24 reflects the high position resolution obtained from the DCs. This distribution contains residuals from hits throughout a drift chamber cell. The resolution within a cell is strongly dependent on the distance from the wire, being poor close to the wire (due to ionization statistics) and improving drastically away from the wire as can be seen from Fig. 26. Away from the wire, resolutions of up to 30 microns have been achieved with the use of DME gas by other

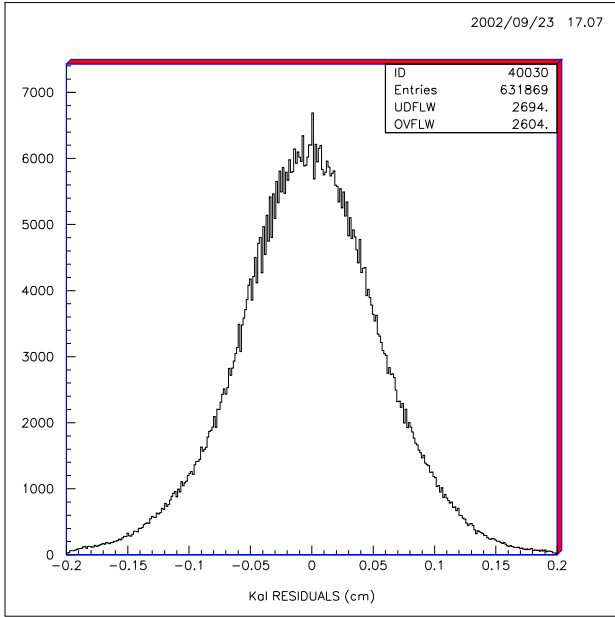


Figure 22: Residuals distribution for straight through tracks before plane alignments and accurate drift times are incorporated.

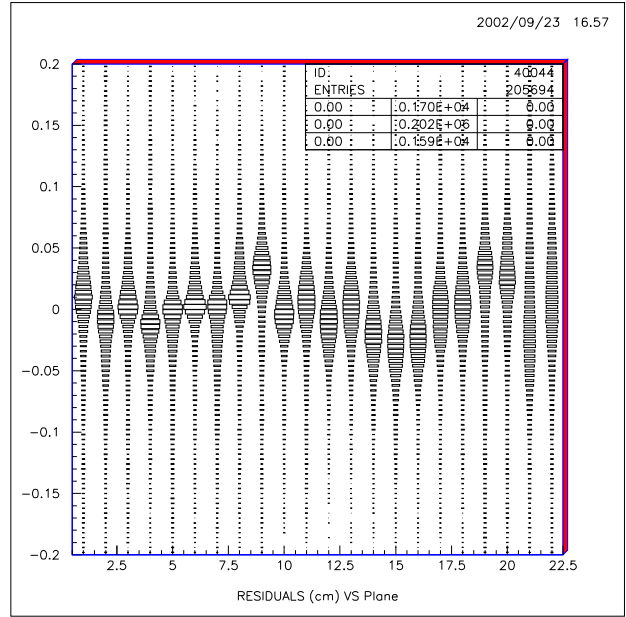


Figure 23: Residuals as a function of plane number for all 44 DC planes before plane alignments are determined.

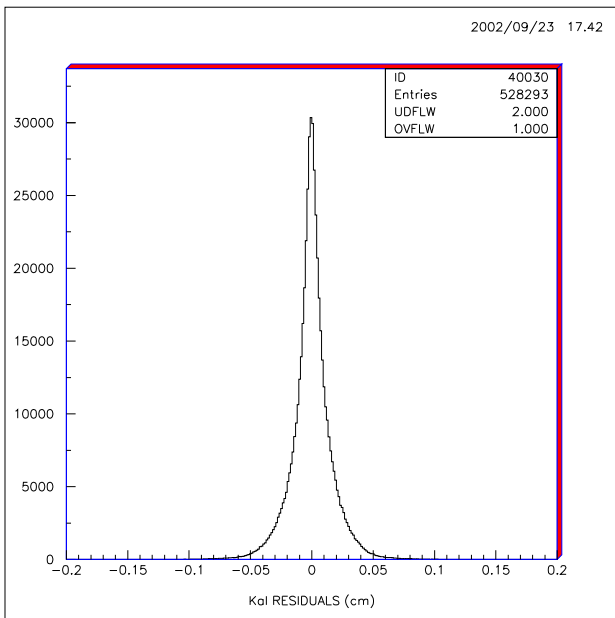


Figure 24: Residuals distribution for straight through tracks after plane alignments and accurate drift times are incorporated.

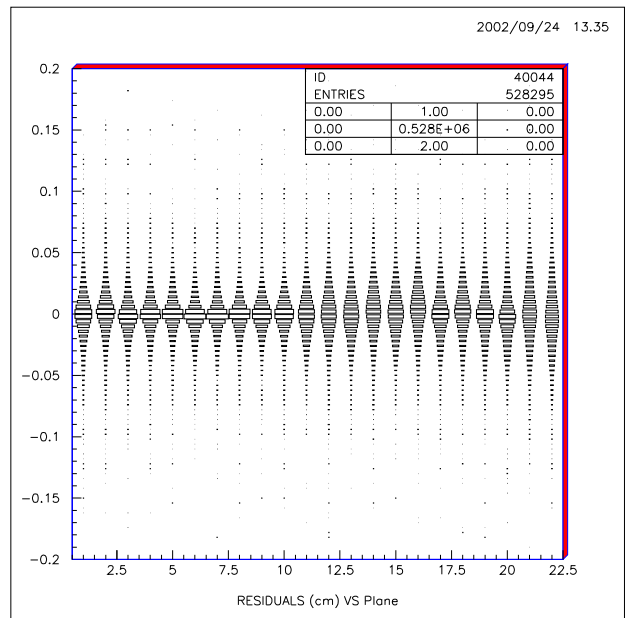


Figure 25: Residuals as a function of plane number for all 44 DC planes after plane alignments are determined.

groups. With further improvements in the various chamber calibrations, TWIST should be able to obtain similar resolutions.

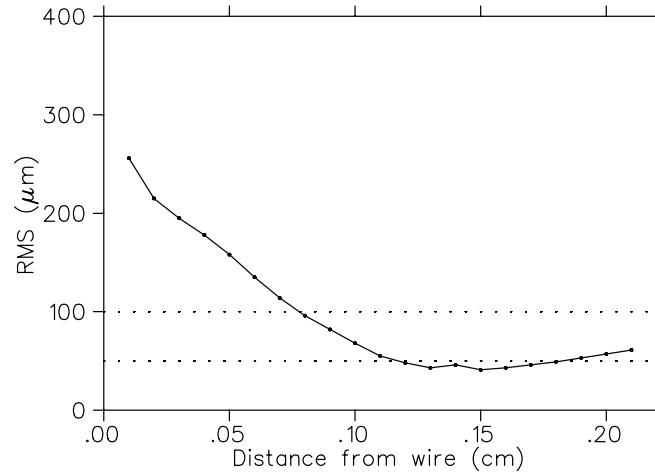


Figure 26: Resolution *vs* distance from wire.

5.2 Preliminary results

Considerable progress was made in the past year to modify and test the pattern recognition code. The pattern recognition code utilizes information collected from the various detectors and classifies the event accordingly. Such classifications include a clean decay event where the hit patterns are not ambiguous and consistent with a muon stopping in the target followed by a positron coming out of the target, events in which a clean decay is obscured by a beam particle, events accompanied by the emission of a delta ray, and track kinks caused by a hard scatter.

Since the event selection process might result in energy or angle biases if events are misclassified, it is vital that this code be tested on Monte Carlo events. Various studies are now in progress aimed at testing the efficiency of event classification. In particular, the capability of generating beam positrons together with muons have been added to the *TWIST* Monte Carlo, which will aid in testing the performance of the pattern recognition code under such circumstances. Several tests are also in progress to evaluate the ability of the pattern recognition code to identify deltas, and to test whether the identification efficiency is energy and/or angle dependent.

Particle identification techniques are also being developed and tested; these techniques use analogue (PACT) information, as well as hit patterns in the chambers.

In addition, the pattern recognition code uses time windows created from PC timing information to classify the TDC hits. The classification is further refined by attempting to verify that hits in a specific window are indeed consistent with a given track using a crude (but CPU efficient) reconstruction technique. A vast amount of effort has been invested in testing and refining these techniques using real as well as Monte Carlo data.

Systematic studies are being conducted to evaluate the effect of beam rate on event classification and reconstruction and, subsequently, the Michel distribution. Two significant data sets were taken during the abbreviated summer 2002 run, at muon counter rates of 2 kHz and 4 kHz. Additionally, low statistics were accumulated for six settings of muon counter rates between 0.88 kHz and 6.3 kHz. Monte Carlo runs have been produced using identical conditions. Ongoing studies are looking at the number and percentage of selected events as a function of beam rate for both Monte Carlo and data. Further studies are looking at the track reconstruction efficiency.

Data were taken in August 2002 to help validate delta production in GEANT. These data included a series of runs acquired with a positron beam with the beam tuned at several different momenta from 30 to 50 MeV/c and purposely misaligned to result in a large transverse momentum. Another series of runs with a surface muon beam was acquired where material of different types and thicknesses were placed at the downstream end of the detector, to compare with the simulation and determine the consequence of a source of backscattering of decay positrons.

Progress has also been made on the final χ^2 fitting code. Helix parameters obtained from the crude pattern recognition fit are used as a starting point for the helix fit. The helix fit proceeds to fine-tune these parameters by incorporating drift time information as well as correct fit weights that incorporate multiple scattering. The code then proceeds to calculate the energy and emission angle of the decay positron. Detailed testing of this code on both data and Monte Carlo is underway. Figure 27 shows the muon decay curve, while Fig. 28 shows a sample Michel spectrum of the positron energy from muon decay.

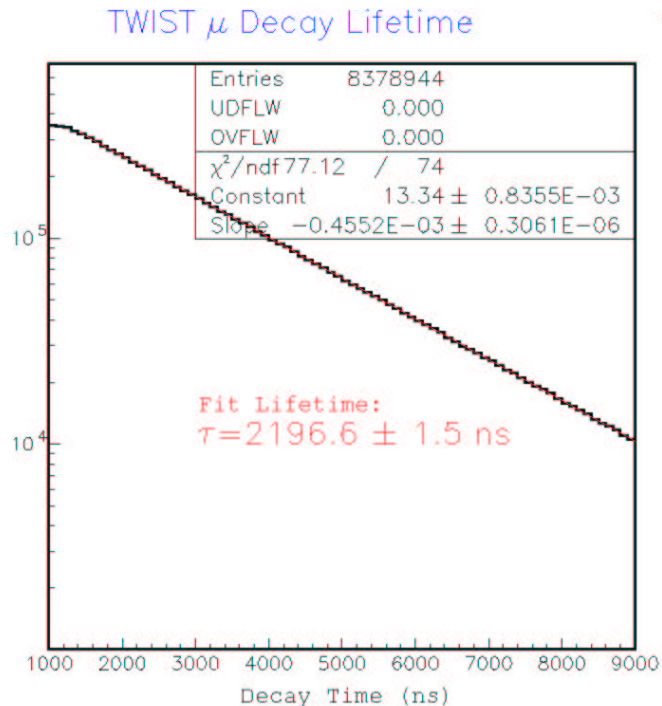


Figure 27: Muon lifetime fit from *TWIST* data.

6 Summary

The *TWIST* project, and Canadian subatomic scientists in general, suffered a very tragic loss in 2002 with the passing of Prof. Nathan Rodning. Nate was an enthusiastic and energetic supporter of *TWIST*, of his students and colleagues, and of the value of science to our life and culture. As *TWIST* collaborator and project leader for several years, he worked tirelessly to bring the experiment to the point at which it is today.

Twist has begun to take high quality data that will submit the Standard Model to several tests. Some systematics study data have been taken and are under analysis. Data sets will be taken in the fall of 2002 to determine ρ and δ to an initial uncertainty of 10^{-3} , with results expected as early as mid 2003. However, we do not yet have all the ingredients necessary for the full and successful completion of our program. For example, we still have to build a device such as the time expansion chamber (TEC) in order to provide the best possible beam characteristics, especially for a measurement of $P_\mu \xi$. In addition, it is clear that the challenge of understanding the systematics fully, of continuing to test the validity of our Monte Carlo under realistic conditions, and of analyzing the substantial amounts of data expected, would best be

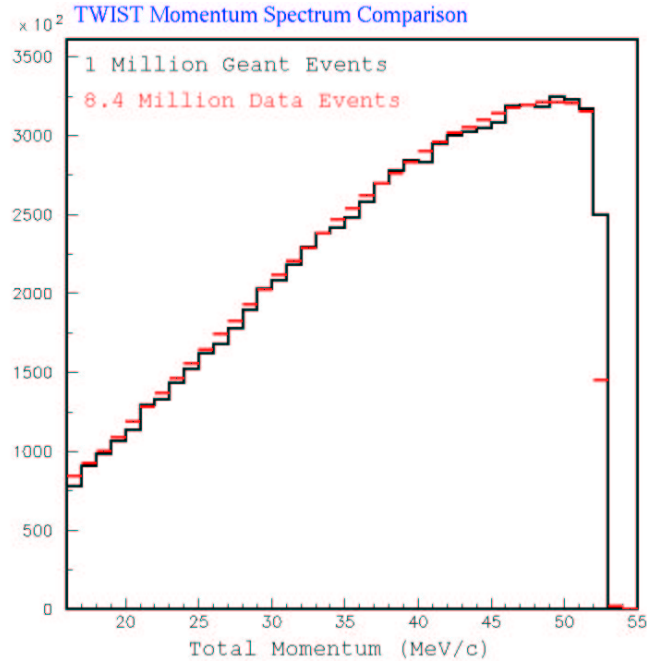


Figure 28: Preliminary comparison with Monte Carlo energy distribution.

met with a modest increase in our numbers of research associates and students, along with the foreseen increased involvement of the Regina group. The substantial majority of the equipment has been constructed, assembled, and tested, and so far the *TWIST* spectrometer has shown that it can deliver what we expect of it. We look forward to several years of data taking and analysis; no doubt there will be some surprises, but there will most certainly be good science.

References

- [1] L. Michel, Proc. Phys. Soc. **A63**, 514 (1950).
- [2] W. Fetscher, H.-J. Gerber, and K. F. Johnson, Phys. Lett. **B173**, 102 (1986).
- [3] Particle Data Group, Phys. Rev. **D66**, 1 (2002).
- [4] P. Herczeg, Phys. Rev. **D34**, 3449 (1986).
- [5] D0 Collaboration, S. Abachi *et al.*, Phys. Rev. Lett. **76**, 3271 (1996).
- [6] D. Acosta *et al.*, Search for a W' Boson Decaying to a Top and Bottom Quark Pair in 1.8 TeV $p\bar{p}$ Collisions, arXiv:hep-ex/0209030 (CDF/PUB/EXOTIC/PUBLIC/5927), 2002.
- [7] A. Jodidio *et al.*, Phys. Rev. **D34**, 1967 (1986).
- [8] A. Jodidio *et al.*, Phys. Rev. **D37**, 237 (1988).
- [9] K. S. Babu and S. Pakvasa, Lepton Number Violating Muon Decay and the LSND Neutrino Anomaly, arXiv:hep-ph/0204236 (OSU-HEP-02-05), 2002.
- [10] J. Peoples, Ph.D. thesis, Columbia University, 1966.
- [11] B. Balke, Ph.D. thesis, University of California, Berkeley, 1987.
- [12] D. Stoker, Ph.D. thesis, University of California, Berkeley, 1985.
- [13] R. Veenhof, *GARFIELD, A Drift-Chamber Simulation Program, User's guide, ver 7.04*, CERN, 2001.
- [14] J. Groh, E. Schenuit, and H. Spitzer, Nucl. Inst. and Meth. **A293**, 537 (1990).
- [15] M. Berger and S. Seltzer, Tables of Energy Losses and Ranges of Electrons and Positrons, Publication 1133, National Academy of Sciences (National Research Council, Washington, DC), 1964.
- [16] M. Berger, Electron Stopping Powers for Transport Calculations, in Monte Carlo Transport of Electrons and Photons, ed. T.M. Jenkins, W.R. Nelson and A. Rindi, Plenum Press, 1986.
- [17] R. Openshaw *et al.*, Tests of Wire Chamber Ageing with CF₄/Isobutane (80:20), Argon/Ethane (50:50), and Argon/Ethane/CF₄ (48:48:4), in Nuclear Science and Nuclear Power Systems, IEEE T-NS-36/1, p. 567, 1989.
- [18] D. G. Fleming and M. Senba, Atomic Physics with Positrons, ed. J.W. Humberston and E.A.G. Armour, Plenum, 1987.